

X-ray Binaries in External Galaxies

Marat Gilfanov ^{*}, Giuseppina Fabbiano, Bret Lehmer and Andreas Zezas

Abstract X-ray appearance of normal galaxies is mainly determined by X-ray binaries powered by accretion onto a neutron star or a stellar mass black hole. Their populations scale with the star-formation rate and stellar mass of the host galaxy and their X-ray luminosity distributions show a significant split between star-forming and passive galaxies, both facts being consequences of the dichotomy between high- and low-mass X-ray binaries. Metallicity, IMF and stellar age dependencies, and dynamical formation channels add complexity to this picture. The numbers of high-mass X-ray binaries observed in star-forming galaxies indicate quite high probability for a massive star to become an accretion powered X-ray source once upon its lifetime. This explains the unexpectedly high contribution of X-ray binaries to the Cosmic X-ray Background, of the order of $\sim 10\%$, mostly via X-ray emission of faint star-forming galaxies located at moderate redshifts which may account for the unresolved part of the CXB. Cosmological evolution of the $L_X - \text{SFR}$ relation can make high-mass X-ray binaries a potentially significant factor in (pre)heating of intergalactic medium in the early Universe.

Marat Gilfanov
Max-Planck-Institute for Astrophysics, Garching, Germany and Space Research Institute, Moscow, Russia,
e-mail: gilfanov@mpa-garching.mpg.de

Giuseppina Fabbiano
Harvard-Smithsonian Center for Astrophysics (CfA), Cambridge MA, USA,
e-mail: gfabbianocfa.harvard.edu

Bret Lehmer
University of Arkansas, USA
e-mail: lehmer@uark.edu

Andreas Zezas
University of Crete, Crete, Greece,
e-mail: azezas@physics.uoc.gr

^{*} corresponding author

Keywords: X-ray binaries, black holes, neutron stars, ultra-luminous X-ray sources, X-ray populations, metallicity dependence, X-ray scaling relations, accretion, preheating of IGM

1 Introduction

X-ray binaries (XRBs) are binary stellar systems composed of a relativistic compact object – a neutron star (NS) or a black hole (BH), and a stellar companion. They are powered by accretion of matter from the donor star onto the compact object (Shakura & Sunyaev, 1973) and are the most common luminous compact X-ray sources in the Milky Way (see Lewin et al. 1995; Lewin & van der Klis 2006; Gilfanov 2010 for a review). While some luminous XRBs were detected in the early days of X-ray astronomy in Local Group galaxies, it was only after the deployment of the first imaging X-ray telescope, the Einstein Observatory in 1978, that their presence as ubiquitous populations of X-ray sources in galaxies could be established (see Fabbiano 1989 for a review). A number of individual XRBs were resolved with Einstein in the more nearby galaxies (e.g. van Speybroeck et al., 1979; Long & van Speybroeck, 1983), leading to the first attempts at characterizing these populations with luminosity functions (see Fabbiano 1988 for a M81 – M31 comparison). These individual detections included a new class of very luminous X-ray sources emitting in excess of the Eddington luminosity limit of a ~ 10 solar mass accreting object (Long & van Speybroeck, 1983), now known as ultraluminous X-ray sources (ULXs).

X-ray emission was detected from over 230 galaxies of all morphological types covered by the Einstein field of view, resulting in the publication of the Einstein Catalog of Galaxies (Fabbiano et al., 1992). Studies of the Local Group galaxies led to the realization that different XRB populations reside in galaxies (e.g. Long & van Speybroeck, 1983; Helfand, 1984), akin to those in the Milky Way (cf Grimm, Gilfanov, & Sunyaev, 2002). For more distant galaxies, Einstein and, a decade later, ROSAT Observatory, could not yet resolve compact X-ray populations to the sufficient depth and detail, however, meaningful correlations were found between integrated X-ray emission and various multiwavelength tracers such as optical, near- and far-infrared and radio emission (David, Jones, & Forman, 1992; Fabbiano & Shapley, 2002). These discoveries led to formulation of many elements of the overall picture of X-ray binary populations in galaxies. It was realised, in particular, that young XRB population, identified with high-mass X-ray binaries (HMXBs), is prevalent in the arms of spiral galaxies and in late-type systems with young stellar population and more intense star formation rate. An older population of low-mass X-ray binaries (LMXBs) is instead found in the older galaxy disks and in the bulges.

Following the demise of the Einstein Observatory, the study of galaxies was continued with other X-ray telescopes (ROSAT, ASCA, XMM-Newton). However, the real new breakthroughs in the study of the XRB populations have only occurred thanks to the deployment of the Chandra X-ray Observatory (Weisskopf et al.,

2000). With its sub-arcsecond angular resolution, Chandra has revolutionized this field, leading to the widespread detection of rich populations of XRBs in galaxies well outside the Local Group (see reviews (Fabbiano, 2006, 2019; Gilfanov, 2004)).

In this Chapter we give an overview of the contemporary understanding of populations of XRBs in external galaxies and of their properties. The following discussion is mostly based on the results of Chandra observations. For the comprehensive review of earlier findings we refer the reader to (Fabbiano, 1989).

2 High- and low-mass X-ray binaries

Depending on the mass of the optical companion, X-ray binaries are broadly divided into two classes – high- and low- mass X-ray binaries (HMXBs and LMXBs), separated by a thinly populated region between $\sim 1 M_{\odot}$ and $\sim 5 M_{\odot}$, where bright persistent X-ray sources are scarce, for the reasons discussed in Section 7. The difference in the mass of the donor star determines the difference in the formation time scales of these two classes of X-ray binaries, which are governed by a combination of the nuclear timescale of the donor stars and the time required for the onset of mass transfer from the donor star to the compact object.

In the case of an HMXB, this timescale is determined by the nuclear evolution of the massive donor star. Correspondingly, they are X-ray bright within ~ 100 Myrs after formation of the binary system (e.g. Verbunt & van den Heuvel, 1995). This is comparable to the characteristic timescale of the star-formation episode, therefore one may expect that the number of such systems in a galaxy is proportional to its star-formation rate (SFR) (Sunyaev, Tinsley, & Meier, 1978; Grimm, Gilfanov, & Sunyaev, 2003; Mineo, Gilfanov & Sunyaev, 2012):

$$N_{\text{HMXB}}, L_{\text{X,HMXB}} \propto \text{SFR} \quad (1)$$

Evolution of primordial LMXBs is determined by the rate of loss of the orbital angular momentum of the binary system or by the nuclear evolution of the low-mass star, both of which, on the contrary to prompt HMXBs, are typically in the $\sim 1 - 10$ Gyrs range (Verbunt & van den Heuvel, 1995). Correspondingly, one may expect that their population integrates the long-term star-formation history of the host galaxy and scales with the total mass of its stars (Gilfanov, 2004):

$$N_{\text{LMXB}}, L_{\text{X,LMXB}} \propto M_{*} \quad (2)$$

LMXBs can be also formed dynamically in globular clusters and galactic nuclei which complicates this simple picture; this is discussed in Section 5.

3 X-ray scaling relations and luminosity functions

3.1 *Disentangling HMXB and LMXB populations in external galaxies*

High- and low-mass X-ray binaries scale, respectively, with the SFR and stellar mass of their parent stellar populations (Section 2). They also share different evolutionary paths (e.g. Tauris & van den Heuvel, 2023). For these reasons it is often useful to discriminate between the two classes in observations.

With the exception of a few nearby galaxies (for example Magellanic Clouds; e.g. Antoniou et al., 2010; Haberl et al., 2012; Shtykovskiy & Gilfanov, 2005a,b) or a few detailed HST-based studies (e.g. Garofali et al., 2018), it is extremely difficult to determine the nature of the donor star in galaxies located beyond ~ 1 Mpc, which would allow us to directly discriminate between high- and low-mass X-ray binaries.

However, given that HMXBs are fueled by short-lived early-type OB stars, they become extinct after a few hundred million years after their formation. Therefore, old stellar environments are populated by LMXBs. Similarly, young stellar environments are dominated by HMXBs, (a) because of the much higher formation efficiency of HMXBs (e.g. Antoniou et al., 2019; Mineo, Gilfanov & Sunyaev, 2012) (Section 7.3), and (b) because LMXBs did not have the time to form in environments much younger than \sim Gyr. Therefore, we can use estimates of relative fractions of old and young stellar populations in a galaxy to disentangle populations of HMXBs and LMXBs. A commonly used proxy for assessing the dominant XRB population is the specific SFR (sSFR) defined as the ratio of the SFR over the stellar mass at the same region of a galaxy. Generally, regions with sSFR higher than $\sim 10^{-10}\text{yr}^{-1}$ are dominated by HMXBs (Grimm, Gilfanov, & Sunyaev, 2003; Mineo, Gilfanov & Sunyaev, 2012; Lehmer et al., 2010), whereas $\text{sSFR} \leq 10^{-11}\text{yr}^{-1}$ would suggest an LMXB-dominated environment, although these thresholds can vary depending on the recent star-formation history of the galaxy.

3.2 *X-ray scaling relations.*

Chandra X-ray observatory presented an opportunity to observe compact sources in galaxies located at distances up to $\sim 30 - 50$ Mpc (and more for the brightest sources) in a nearly confusion-free regime, to measure their luminosity functions and total luminosities of different (sub)populations. Observations of a large number (\sim hundred) of nearby galaxies have demonstrated that populations of LMXBs and HMXBs in a galaxy scale proportionally to its stellar mass and SFR respectively (Fig. 1):

$$L_{X,\text{HMXB}} \approx 2.6 \cdot 10^{39} \times \text{SFR} \quad N_{\text{HMXB}} \approx 10 \times \text{SFR} \quad (3)$$

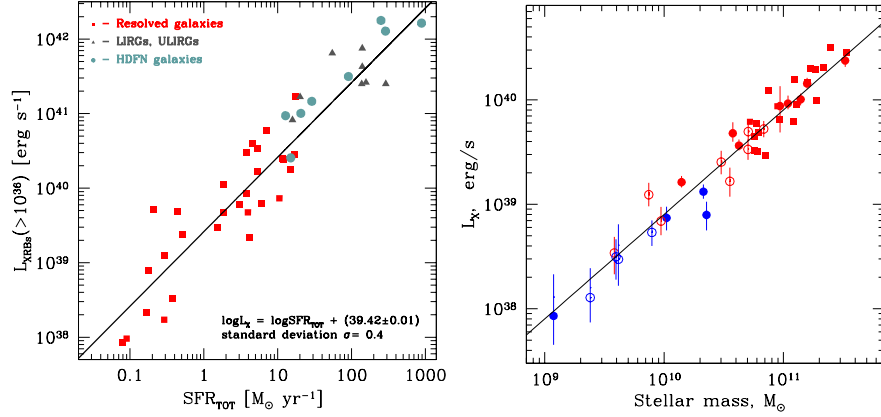


Fig. 1 Dependence of the total X-ray luminosity of X-ray binaries on the SFR (left panel) and stellar mass (right panel) of the host galaxy. Left panel shows star-forming galaxies, young stellar population of which is dominated by massive X-ray binaries; their population is roughly proportional to the SFR of the host galaxy. Right panel shows data for elliptical galaxies where star-formation mostly stopped at least several Gyrs ago and only low-mass X-ray binaries are left. Their population is determined by the total stellar mass of the host galaxy. Solid lines show approximation of the data by the linear laws. In the left panel we also show the data for ultra-luminous infrared galaxies (ULIRGs, triangles) and star-forming galaxies from the Chandra Deep Fields. These galaxies are not resolved by Chandra, therefore the total luminosity is shown, including contribution of faint unresolved compact sources and diffuse emission. Adapted from (Gilfanov, 2004; Mineo, Gilfanov & Sunyaev, 2012; Zhang, Gilfanov & Bogdan, 2012).

$$L_{X,\text{LMXB}} \approx 10^{39} \times \frac{M_*}{10^{10} M_\odot} \quad N_{\text{LMXB}} \approx 14 \times \frac{M_*}{10^{10} M_\odot} \quad (4)$$

where L_X is the total X-ray luminosity of X-ray binaries of the given type in the 0.5–8 keV energy band, N_X the number of X-ray binaries with luminosity exceeding $L_X \geq 10^{37}$ erg/s, SFR is the star-formation rate in M_\odot/yr , and M_* is the stellar mass of the galaxy in solar units (Grimm, Gilfanov, & Sunyaev, 2003; Mineo, Gilfanov & Sunyaev, 2012; Gilfanov, 2004). Broadly consistent results were obtained in several other independent studies (e.g. Ranalli, Comastri, Setti, 2003; Colbert et al., 2004; Kim & Fabbiano, 2004; Lehmer et al., 2010; Sazonov & Khabibullin, 2017). However, there is a caveat to keep in mind when comparing different scaling relations. The coefficients in eq.(3), (4) depend first of all on the methods used for estimating the stellar mass and SFR, their proxies and assumed shape of the initial mass function (IMF). This is illustrated by Fig. 2 and explained later in this section. Secondly, they depend on the particular samples of galaxies, their age and star-formation history composition, metallicity, globular cluster content, etc. Various aspects of these dependencies are discussed in the following sections of this chapter.

The $L_X - \text{SFR}$ relation is subject to a curious statistical effect, making it to appear steeper than linear and to have large dispersion at low SFR (Grimm, Gilfanov, & Sunyaev, 2003; Gilfanov, Grimm, & Sunyaev, 2004). This behavior is caused by the poor sampling of the bright luminosity end of the X-ray luminosity function (XLF)

at low SFR and its magnitude depends on the XLF shape, in particular its slope and position of the high luminosity cut-off (Gilfanov, Grimm, & Sunyaev, 2004). It is much more pronounced for HMXBs because of their relatively flat XLF and is insignificant for LMXBs which XLF is steep at the high luminosity end (Section 3.3). Note that this effect is not seen in Fig. 1 because of the observer bias (Mineo, Gilfanov & Sunyaev, 2012).

In order to account for the HMXB and the LMXB components simultaneously Lehmer and collaborators (Lehmer et al., 2010) introduced a scaling relation of the form

$$L_X = \beta \text{SFR} + \alpha M_* \quad (5)$$

An equivalent form in terms of specific SFR is also often used:

$$L_X/\text{SFR} = \beta + \alpha \times \text{sSFR}^{-1} \quad (6)$$

Lehmer et al. (2019) derived values of the scaling parameters: $\log \alpha [\text{erg s}^{-1} M_\odot^{-1}] = 29.25_{-0.06}^{+0.07}$ and $\log \beta [\text{erg s}^{-1} (M_\odot \text{ yr}^{-1})^{-1}] = 39.71_{-0.09}^{+0.14}$. Their best fit to the data is shown in Fig. 2. This parameterization allows one to combine the contribution of the LMXB and HMXB components in a single formulation, and it is particularly useful for galaxies with low sSFR such as early-type spiral galaxies that have a significant LMXB component.

The parameters α and β in eq. (6) characterising X-ray scaling relations for LMXBs and HMXBs are in an apparent disagreement with those in eqs. (3) and (4). The disagreement is not real, as discussed earlier in this section, it is caused by the differences in the assumed IMF and proxies used for the SFR and stellar mass estimations in the different analyses. When they are taken into account (Lehmer et al., 2019), the scaling relations from Gilfanov (2004); Mineo, Gilfanov & Sunyaev (2012); Zhang, Gilfanov & Bogdan (2012); Lehmer et al. (2019) are fully consistent with with each other as it is illustrated in the right panel in Fig. 2.

3.2.1 Time dependence of HMXB population

Scaling relations in Fig. 1 and 2 are drawn for quantities integrated over entire galaxies. As such, they represent a result of averaging over a (typically large) number of star-forming regions. The details regarding ages, metallicities and star-formation histories of the individual star-forming regions are smeared out and such scaling relations characterise populations X-ray binaries globally, on the galactic scales. Spatially resolved analysis of individual galaxies, on the other hand, can reveal a more detailed picture of evolution of the population of HMXBs with time after their formation.

A particularly promising way is to compare the spatial distribution of HXMBs in a galaxy with its spatially resolved star-formation history or the stellar population age. At present, this can be done only for the handful of the most nearby galaxies, and the results are limited by the statistical quality of the available data, in partic-

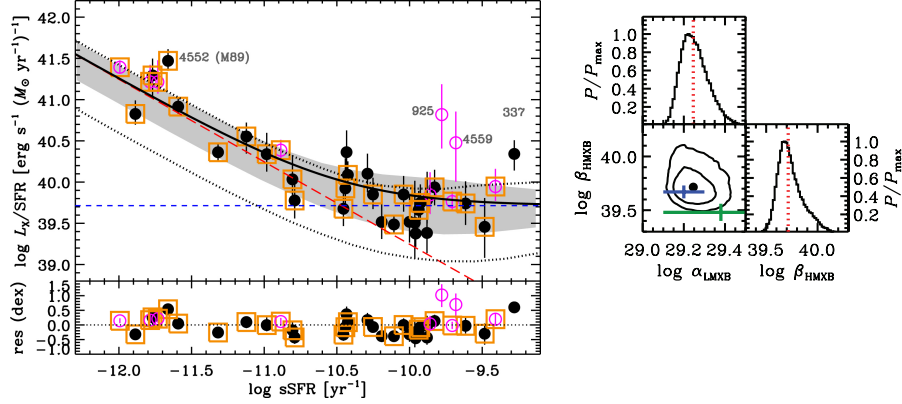


Fig. 2 *Left*: Dependence of the total X-ray luminosity per unit SFR on the sSFR of the host galaxy. The red-dashed line indicates the contribution from LMXBs, while the blue-dashed line indicates the contribution from HMXBs. Galaxies with sSFR greater than ($\sim 10^{-10.5} M_{\odot} \text{yr}^{-1} M_{\odot}^{-1}$) are dominated by HMXBs while at lower values of sSFR the contribution of LMBXBs becomes increasingly more important. The gray shaded region and the dotted lines delineate the 1σ scatter resulting from uncertainties in the XLF of the resolved X-ray binaries for galaxies with median mass of $2 \times 10^{10} M_{\odot}$, and $3 \times 10^9 M_{\odot}$. *Right*: Comparison of scaling parameters α_{LMXB} and β_{HMXB} from eq. (6) derived in Lehmer et al. (2019) (MCMC contours) with those from eqs. (3) and (4) (Gilfanov, 2004; Mineo, Gilfanov & Sunyaev, 2012; Zhang, Gilfanov & Bogdan, 2012) (blue cross with corresponding 1σ errors) after differences in assumed IMF and SFR, M_* proxies are taken into account. The green cross shows the Chandra Deep Field-South independent estimates from Lehmer et al. (2016). See Lehmer et al. (2019) for more details. Adapted from Lehmer et al. (2019).

ular, by the number of HMXBs and fairly poor sampling of their parameter (type, luminosity etc) space.

In the case of the Magellanic Clouds comparison of the X-ray binary populations with the star-formation history (SFH) of their parent stellar populations permitted the authors to reconstruct the HMXB formation efficiency $\eta_{\text{HMXB}}(\tau)$ (see definition in Shtykovskiy & Gilfanov, 2007) and the age distribution of HMXBs as shown in Fig. 3. It was shown that there is a peak at their formation efficiency at $\sim 30 - 60$ Myr, consistent with increased formation of Be stars at the same timescales (Shtykovskiy & Gilfanov, 2007; Antoniou et al., 2010; Antoniou & Zezas, 2016; Antoniou et al., 2019). As it should have been expected, the peak in the population of HMXBs is delayed with respect to the peak in the formation rate of compact objects (left and middle panels in Fig. 3). The magnitude of the delay is determined by the time required to form the compact object (mostly neutron stars in the case of HMXBs in Magellanic Clouds) and for the nuclear evolution of the secondary star. These results give a formation rate of ~ 1 X-ray binary per 200 observed stars of OB spectral types at ages of $\sim 30 - 60$ Myr, or equivalently ~ 9 XRBs per $10^6 M_{\odot}$ of stars formed at a star-formation episode, which agrees very well with the theoretical models, as one can see in the left panel in Fig. 3 (see also Fig. 4)

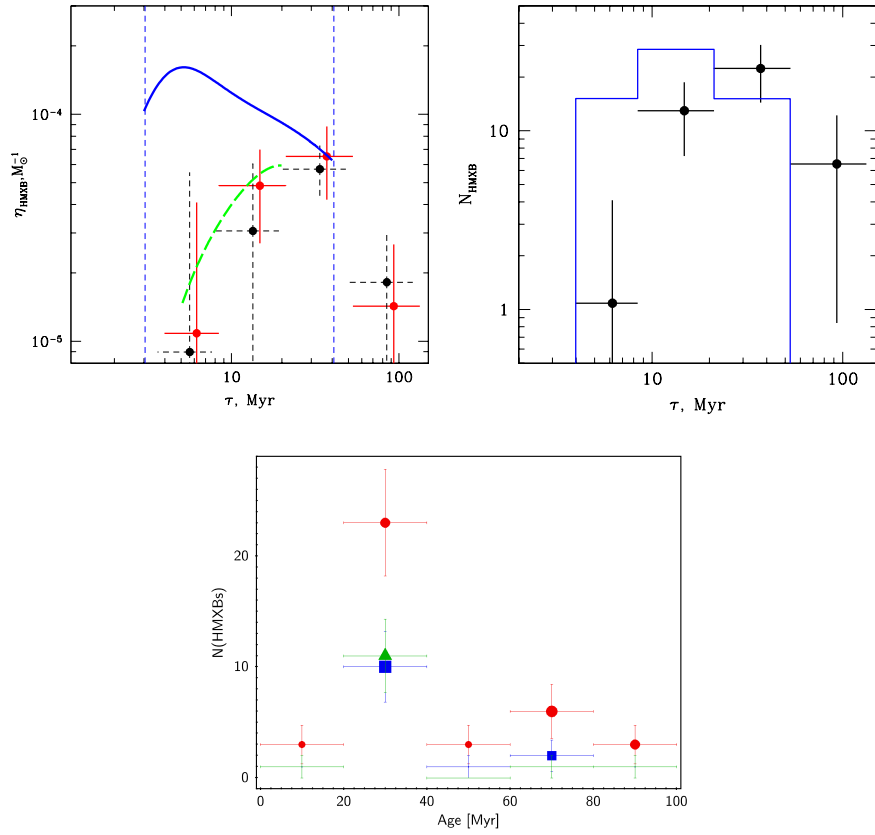


Fig. 3 *Top-left panel:* Dependence of the HMXB number on the time elapsed since the star formation event. The solid and dashed crosses were obtained using different reconstructions of spatially resolved star-formation histories (see Shtykovskiy & Gilfanov (2007) for details). The solid curve shows the type II supernova rate. The two vertical dashed lines mark formation times of the first black hole and the last neutron star calculated in the standard theory of evolution of a single star. The dashed curve represents the theoretical dependence of the number of Be/X systems with neutron stars from Popov et al. (1998). *Top-right panel:* The age distribution of HMXBs in the SMC. The solid histogram shows the distribution expected if HMXB numbers followed the core collapse supernova rate. The top panels adapted from Shtykovskiy & Gilfanov (2007) *Bottom panel:* The age distribution of HMXBs in the LMC. Adapted from Antoniou & Zezas (2016)

Magellanic Clouds have fairly low star-formation rates and their X-ray populations are dominated by low luminosity sources (e.g. Gilfanov, Grimm, & Sunyaev, 2004). The $\eta_{\text{HMXB}}(\tau)$ shown in Fig. 3 describes X/Be systems which these galaxies are populated with, hence it peaks at \sim several tens of Myrs. Similar analysis for high-SFR galaxies (e.g. Antennae or Cartwheel) would reveal a complex picture of the formation efficiencies and time scales depending on X-ray luminosity. In particular one might expect to see that $\eta_{\text{ULX}}(\tau)$ for ultra-luminous X-ray sources peaks at much earlier times. However, such analysis would require to resolve stellar populations and to derive spatially resolved star-formation histories at distances of $\sim 10 - 100$ Mpc.

3.2.2 Metallicity and age effects

X-ray binary population synthesis models (e.g. Fragos et al., 2013; Linden et al., 2010) showed that the number of X-ray binaries, the shape of their luminosity function, and their integrated X-ray luminosity evolve strongly as a function of age and metallicity (Fig. 4). The general trend is that as a stellar population ages the integrated X-ray luminosity of its X-ray binaries declines. In the case of metallicity, lower metallicity stellar populations are associated with higher integrated X-ray luminosities.

These predictions have been confirmed from studies of the X-ray luminosity or the number of X-ray binaries as a function of the age of the stellar populations (e.g. Lehmer et al., 2019). Similarly, studies of the effect of metallicity showed strong anti-correlation of the integrated X-ray luminosity of galaxies and their metallicity (see discussion in section 8.4 and Fig. 13) (e.g. Brorby et al., 2016; Prestwich et al., 2013; Mapelli, Colpi, & Zampieri, 2009; Lehmer et al., 2016). Such behaviour is attributed to the weaker stellar winds of low-metallicity stars, resulting in tighter orbits at the start of the X-ray emitting phase, and hence higher probability of systems undergoing Roche-lobe overflow (e.g. Linden et al., 2010). Metallicity dependence is further discussed in Section 8 in the context of cosmic evolution of X-ray binary populations in galaxies.

3.2.3 Sub-galactic scales

Sub-galactic scales open a window into the complex picture of evolving X-ray populations (Section 3.2.1) however require adequate angular resolution and sensitivity to properly resolve optical and X-ray populations. At present, beyond the Local Group, one can only study behaviour on \sim few kpc scales of integrated (unresolved) X-ray luminosity and various SFR and mass proxies.

Recent studies of the X-ray luminosity, stellar mass and SFR scaling relations in sub-galactic scales as small as 1 kpc^2 showed that unresolved X-ray luminosity follows the same qualitative trends as the galaxy-wide scaling relations Kouroumpatzakis et al. (2020). For larger sub-galactic regions of the $\sim 3 - 4$ kpc size and SFR

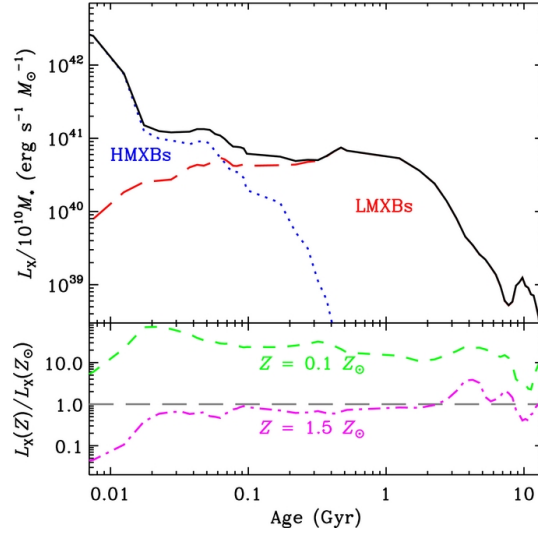


Fig. 4 The evolution of the X-ray luminosity of an initial stellar population of $10^6 M_{\odot}$ as a function of age. The bottom panel shows the ratio of the same model for sub-solar ($0.1 Z_{\odot}$) and supersolar ($1.5 Z_{\odot}$) metallicity with respect to the solar metallicity model. Adapted from (Fragos et al., 2013).

in excess of $\sim 10^{-2} M_{\odot} \text{yr}^{-1}$, correlations of $L_X - \text{SFR}$ converge to the integrated galactic emission relations. In regions of smaller size and/or with extremely low SFR ($< 10^{-2} M_{\odot} \text{yr}^{-1}$) the X-ray luminosity SFR relation shows a flattening which can be attributed to the contribution of the increasingly important LMXB component and, possibly, intrinsically fainter X-ray populations (e.g. active binaries and cataclysmic variables). In addition these sub-galactic relations show significant scatter which is the result of stochastic effects (see Section 3.2) and variations of the stellar populations between different regions of a galaxy.

3.3 X-ray luminosity functions

Chandra observations of many nearby galaxies showed that X-ray luminosity functions of their compact X-ray sources have quite similar shape (Fig.5, right panel), with much stronger variations in normalization than in shape (Grimm, Gilfanov, & Sunyaev, 2003; Gilfanov, 2004; Mineo, Gilfanov & Sunyaev, 2012). It was also immediately noticed that shapes of XLFs are different for X-ray populations in star-forming and elliptical galaxies, i.e. for high- and low- mass X-ray binaries (Fig.5, left panel). In agreement with the scaling relations (Section 3.2), normalization of the HMXB and LMXB luminosity functions scale proportionally to the star-formation rate and stellar mass of the host galaxy correspondingly. These Chandra findings led to the conclusion that luminosity distributions of X-ray binaries can

be described, to the first approximation, by the universal luminosity functions of HMXBs and LMXBs (Grimm, Gilfanov, & Sunyaev, 2003; Gilfanov, 2004) (Fig.5). As time went on and Chandra observations sampled the parameter space of galaxies and also their depth increased, this picture was refined, with age, metallicity, globular cluster content playing their roles in shaping the luminosity distributions of HMXBs and LMXBs.

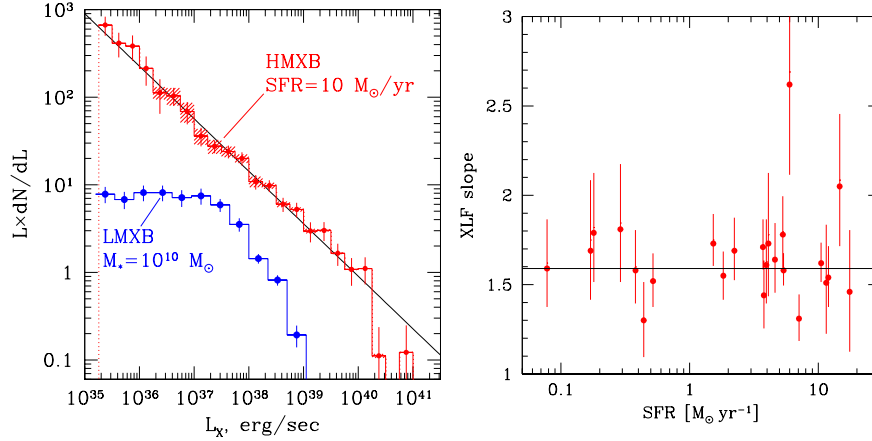


Fig. 5 *Left*: Average X-ray luminosity functions of compact X-ray sources in star-forming (marked "HMXB") and elliptical (marked "LMXB") galaxies. In star-forming galaxies high-mass X-ray binaries dominate, whereas in old elliptical galaxies the dominant component of X-ray populations are low-mass X-ray binaries. Luminosity functions are normalized to star-formation rate of $\text{SFR} = 10 M_{\odot}/\text{yr}$ and stellar mass of $M_{*} = 10^{10} M_{\odot}$ respectively. Based on results of Gilfanov (2004) and Mineo, Gilfanov & Sunyaev (2012). *Right*: XLF slopes for individual star-forming galaxies from the sample of Mineo et al. (Mineo, Gilfanov & Sunyaev, 2012) plotted against the SFR. The solid horizontal line shows the slope of the mean HMXB XLF shown in the left panel. Adapted from Mineo, Gilfanov & Sunyaev (2012).

These refinements added complexity and detail to our understanding of the XLFs of X-ray binaries, but have not changed the fact that the shapes of the XLFs of HMXBs and LMXBs are qualitatively different (Fig.5). The difference is mainly caused by the difference in the mass transfer regime in high and low-mass X-ray binaries (see more detailed discussion in Section 7). Indeed, in the majority of the former the compact object accretes material from the wind of the massive donor star. Their the luminosity function is determined primarily by the mass distribution of the donors in high-mass X-ray binaries (e.g. Postnov, 2003) which leads to the formation of the observed power law luminosity distribution (Grimm, Gilfanov, & Sunyaev, 2003; Mineo, Gilfanov & Sunyaev, 2012):

$$\frac{dN_{\text{HMXB}}}{dL_X} \propto \text{SFR} \times L^{-1.6} \quad (7)$$

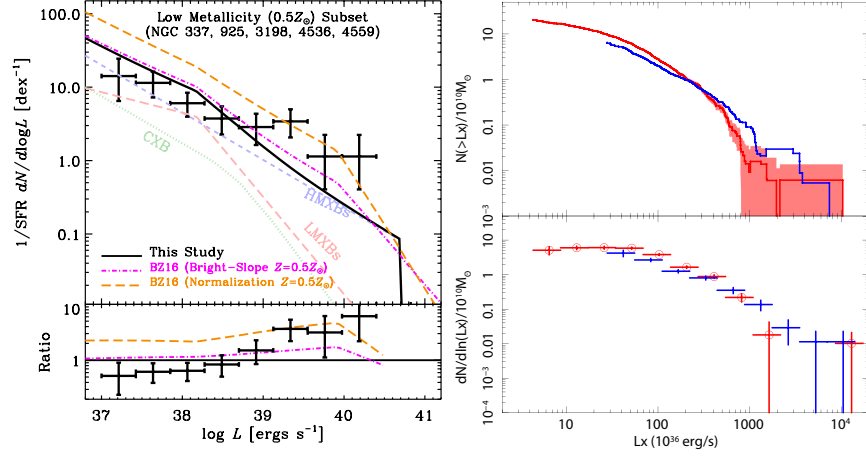


Fig. 6 *Left*: SFR-normalized incompleteness-corrected total XLF for five low metallicity star-forming galaxies (NGC 337, 925, 3198, 4536, and 4559), which have metallicities of $\approx 0.5 Z_{\odot}$. The black curve shows the global model Lehmer et al. (2019) prediction for this population, including HMXB, LMXB, and CXB contributions. Enhancements in the $L \gtrsim 10^{39}$ erg/s source population are clearly observed. The bottom panel shows the ratio of data and population synthesis models with respect to the best-fit global model prediction. Adapted from Lehmer et al. (2019) *Right*: XLFs of LMXBs in young and old galaxies in cumulative (upper panel) and differential (lower panel) forms. See Zhang, Gilfanov & Bogdan (2012) for description of the sample and further details. The data for old galaxies (red) is marked by circles in the lower panel and is surrounded by the shaded area showing the 1σ Poissonian uncertainty in the upper panel. Statistical uncertainty for young galaxies has comparable amplitude. Adapted from Zhang, Gilfanov & Bogdan (2012).

In the case of low-mass X-ray binaries, on the contrary, the mass transfer occurs via donor star Roche lobe overflow through the inner Lagrangian point of the binary system and the X-ray luminosity function of these systems is determined by the orbital parameter distribution of semi-detached binary systems in the galaxy. This leads to formation of the luminosity distribution of a complex shape, with two breaks at $\log L_X \sim 38.5$ and $\log L_X \sim 37 - 37.5$ (Gilfanov, 2004; Kim & Fabbiano, 2010). The first break is located near Eddington luminosity of the neutron star and is likely related with the existence of the luminosity limit for an accreting neutron star – compact objects in more luminous systems are black holes whose occurrence rates in the population are smaller. The nature of the second break is still unclear.

Using large sample of nearby normal galaxies from the Chandra archive, Lehmer and collaborators (Lehmer et al., 2019) analysed XRB populations on sub-galactic scales and built a global XLF model accounting for both types of X-ray binaries and parameterised via SFR and stellar mass of the host galaxy. They found clear transition in XLF shape and normalization per SFR from the almost “pure” HMXB XLF at $sSFR \gtrsim 5 \cdot 10^{-10} \text{ yr}^{-1}$ to the nearly pure LMXB XLF at $sSFR \lesssim 10^{-12} \text{ yr}^{-1}$. The large number of sources (over ~ 4400) in their sample permitted them to accurately describe more subtle XLF features. Also, they found statistically significant evidence that the HMXB XLF in low-metallicity ($\approx 0.5 Z_{\odot}$) galaxies contains an

excess of high luminosity $L_X \gtrsim 10^{39}$ erg/s sources compared to the global average HMXB XLF, which has a median metallicity $\approx Z_\odot$ (left panel in Fig. 6). This result is in line with findings that the integrated X-ray luminosity per SFR is anticorrelated with metallicity (e.g. Basu-Zych et al., 2013; Brorby et al., 2016) and with prediction of the population synthesis modeling (Section 7).

Thanks to their long evolution time scale, in the Gyrs range, time dependence of LMXB populations can be probed with the currently available data. Some dependence on the stellar age is natural to expect, it is predicted in population synthesis modeling (Section 7) and detected in observations (Zhang, Gilfanov & Bogdan, 2012; Lehmer et al., 2019). There is clear evolution of the LMXB XLF with age – younger galaxies have more bright sources and fewer faint ones per unit stellar mass (right panel in Fig. 6). The XLF of LMXBs in younger galaxies appears to extend significantly beyond $\sim 10^{39}$ erg/s. Such bright sources seem to be less frequent in older galaxies.

A natural question is to what degree the variability of the X-ray binary populations affects the shape of the X-ray luminosity function of a given galaxy. Systematic monitoring campaigns on a couple galaxies (the Antennae, M81) showed that while individual sources show significant variability the shape of their X-ray luminosity functions is remarkably stable Zezas et al. (2007). This indicates that a single snapshot of a galaxy can give us a representative picture of its X-ray binary populations.

3.4 X-ray emission as a SFR proxy for normal galaxies

The promptness of HMXBs (Section 3.2.1) makes them a potentially good tracer of the recent star formation activity in a galaxy Sunyaev, Tinsley, & Meier (1978); Ghosh & White (2001). Indeed, existence of correlation of X-ray luminosity of star-forming galaxies with the classical SFR proxy – FIR emission, has been noticed over three decades ago in the Einstein Observatory data (Section 1, refs. Griffiths & Padovani (1990); David, Jones, & Forman (1992)). While there are other sources of X-ray emission in star forming galaxies, such as ionized gas (e.g. Mineo, Gilfanov, & Sunyaev, 2012), in normal galaxies HMXBs dominate and total X-ray emission correlates well with the SFR (Fig. 7).

A multitude of various calibration methods are employed to estimate SFR in external galaxies, based on UV, H_α , FIR or other wavelengths. Any SFR calibrator relies on certain assumptions concerning the environment in the galaxy which lead to various uncertainties e.g. associated with the influence of dust, the escape fraction of photons, the shape of the IMF etc. In fact, many of the commonly used SFR indicators use the signatures of interaction of the ionizing emission from massive stars with the interstellar medium, i.e. may suffer from the same systematic effects. A new independent calibrator is therefore a useful addition to the suite of SFR diagnostics employed by modern astronomy.

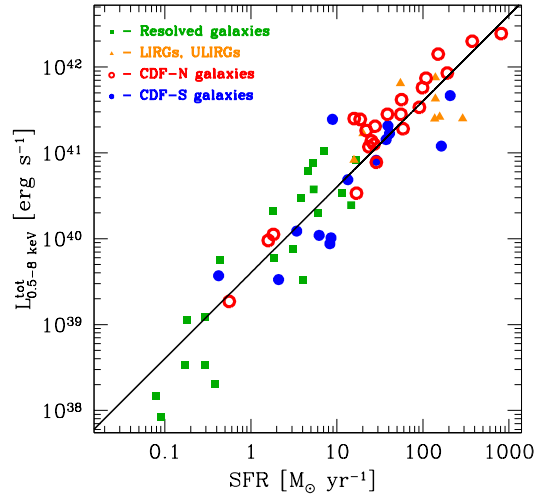


Fig. 7 The relation between SFR and total X-ray luminosity of normal galaxies. The solid line shows the linear scaling relation $L_X = 4 \cdot 10^{39} \times \text{SFR}$. Adapted from Mineo et al. (2014).

A significant advantage of X-ray emission as a diagnostic tool is its large penetrating power – X-rays are much less subject to attenuation by the neutral gas and dust than conventional SFR tracers. Galaxies are mostly transparent to X-rays above ~ 2 keV, except for the densest parts of the most massive molecular clouds. The power law spectra of X-ray binaries are also less susceptible to the effect of the cosmological redshift (K-correction).

The X-ray based SFR proxy, quite naturally, suffers from its own uncertainties and systematic effects. The most important of these is contamination by the activity of supermassive black hole, others are related, for example, to the age and metallicity dependence of the X-ray binary populations. Stochastic effects and variability of the X-ray binaries, makes it less suitable for dwarf galaxies that are dominated by one or two HMXBs. Nonetheless, the X-ray emission of galaxies is a useful and promising proxy of the stellar populations and successfully complements other conventional indicators, particularly in heavily obscured environments. There is a number of its successful applications to reconstruction of the cosmic star formation history (e.g. Aird, Coil, & Georgakakis, 2017; Kurczynski et al., 2012; Norman et al., 2004)

3.5 Expectations from SRG/eROSITA all-sky survey

eROSITA X-ray telescope Predehl et al. (2021) aboard SRG orbital observatory Sunyaev et al. (2021) in the course of its on-going all-sky survey will detect of the order of $\sim 10^4$ normal galaxies out to the distance of a few hundred Mpc

Prokopenko & Gilfanov (2009); Basu-Zych et al. (2020). Although the moderate angular resolution of eROSITA ($\sim 30''$ HPD averaged over the field of view) will not allow for detailed investigations of X-ray populations beyond Local Group, the might of the all sky coverage will make eROSITA data indispensable for detailed investigations of scaling relations and of the patterns of metallicity and age dependence. The main hurdle on this path will be identifying normal galaxies among over 3 million AGN and QSO dominating the eROSITA source catalog (Kolodzig et al., 2013), and isolating the contribution of active nuclei of low luminosity. Significant source of contamination are also X-ray active stars. To this end, multiwavelength data will play a critical role. Galiullin, Gilfanov, Sunyaev (2023) constructed the first SRG/eROSITA – IRAS catalog of X-ray bright star-forming galaxies on the Eastern Galactic sky which currently (after 2 years of sky survey) includes of the order of $\sim 10^3$ star-forming galaxies. With this sample they studied dependence on the SFR and metallicity of the X-ray luminosity of starforming galaxies, separating it into contributions of X-ray binaries and hot inter-stellar medium (ISM) and connecting their finding with the Chandra results described earlier in this section.

4 Spatial distribution of X-ray binaries in galaxies

It was realized since the first X-ray observations of nearby normal galaxies with the Einstein Observatory that the dominant emission above 2 keV – dominated by XRBs - follows that of the stellar surface brightness (see Fabbiano, 1989, and references therein). With its sub-arcsecond angular resolution, Chandra has given us a unique opportunity to explore this connection, for both HMXB and LMXB populations. With Chandra observations XRBs can be individually detected and associate with different galaxy components in the optical band (see Fabbiano, 2006, and references therein).

For the HMXB population, two results are particularly notable: 1) The definitive association of ULXs with star-forming regions, (e.g., in the Antennae (Fabbiano, Zezas, & Murray, 2001), the Cartwheel galaxy (Wolter & Trinchieri, 2004), nearby colliding galaxy pair NGC 2207/IC 2163 (Mineo et al., 2013)), which supports the suggestion that most ULXs may be super-Eddington accreting HMXBs (King et al., 2001; Soria & Ghosh, 2009; Gilfanov & Merloni, 2015). 2) The lack of HMXBs in region of very recent intense star formation, which is consistent with the evolutionary time for a massive binary to reach the HMXB stage. This effect was observed in M51 (Shtykovskiy & Gilfanov, 2007) and the Magellanic Clouds Shtykovskiy & Gilfanov (2005a); Antoniou & Zezas (2016).

The study of the spatial distribution of LMXBs in elliptical galaxies has been motivated by the desire to understand the prevalent formation mechanism for these systems: from the evolution of field binaries, or from dynamical formation in Globular Clusters (GC). In the first case, the radial distribution of LMXB may follow closely that of the stellar light, while in the second it may be more extended. While early studies were inconclusive (see review in Fabbiano, 2006), more recently re-

sults show a possible excess of LMXB at larger radii than expected from the distribution of the optical surface brightness of the galaxies (Zhang, Gilfanov, & Bogdán, 2013; Mineo et al., 2014). This line of investigation is further discussed in Section 5.3.

5 Primordial and dynamically formed LMXBs

5.1 LMXB formation channels

LMXB populations are expected to form through two basic pathways: (1) Roche-lobe overflow of low-mass ($\lesssim 2\text{--}3 M_{\odot}$) donor stars onto compact-object companions in isolated binary systems that form in situ within galactic fields; and (2) dynamical interactions (e.g., tidal capture and multibody exchange with constituent stars in primordial binaries) in high stellar density environments like globular clusters (GCs, Clark & Parkinson, 1975; Fabian, Pringle & Rees, 1975; Hills, 1976) and near the centers of galaxies (e.g., Voss & Gilfanov, 2007b; Zhang et al., 2011). The relative roles of these two channels have been debated. Given the very high formation efficiencies of GC LMXBs (a factor of $\approx 50\text{--}100$ times higher per stellar mass than that of the field), it has been speculated that field LMXB populations may initially form dynamically within GCs, and subsequently “seed” galactic fields through ejection or GC dissolution (e.g., Grindlay et al., 1984; Kremer et al., 2018). *Chandra* observations have shown strong evidence that both formation channels are important, with the normalization of the LMXB XLFs being primarily dependent on the integrated stellar mass, with an additional significant dependence on GC specific frequency (number of GCs per galaxy stellar mass; see, e.g., Gilfanov, 2004; Irwin, 2005; Juett, 2005; Humphrey & Buote, 2008; Kim et al., 2009; Boroson, Kim, & Fabbiano, 2011; Zhang et al., 2011; Lehmer et al., 2020).

The combination of *Chandra* and *Hubble Space Telescope* surveys of relatively nearby ($D \lesssim 30$ Mpc) early-type galaxies have allowed for disentanglement of field and GC LMXB populations through the direct multiwavelength classification of X-ray point sources (e.g., Kim et al., 2009; Voss et al., 2009; Paolillo et al., 2011; Luo et al., 2013; Lehmer et al., 2014, 2020; Mineo et al., 2014; Peacock & Zepf, 2016; Peacock et al., 2017; Dage et al., 2019). Studies of LMXBs directly associated with GCs have revealed that their formation efficacy depends on both local stellar interaction rates and metallicity (see, e.g., Pooley et al., 2003; Sivakoff et al., 2007; Cheng et al., 2018). The most apparent trends appear in observed GC colors, with metal rich, red, GCs hosting a factor of ≈ 3 times more LMXBs compared to metal poor, blue GCs (e.g., Kim et al., 2013); however, no significant variation in the GC LMXB XLF slope is observed as a function of GC metallicity.

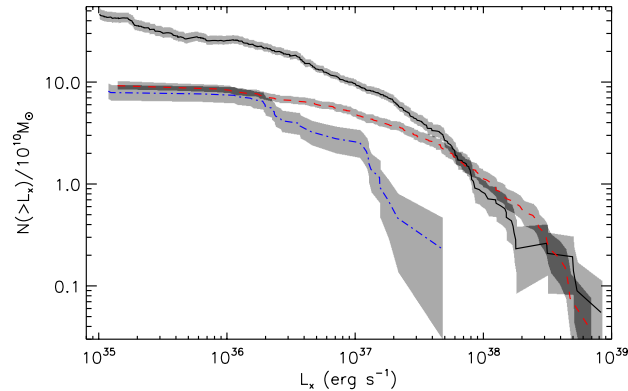


Fig. 8 The stacked XLFs of LMXBs in different environments: field and GC sources in early type galaxies and nucleus of M31. The contribution of CXB sources was subtracted and the incompleteness correction was applied. The field XLF (solid) is normalized to the stellar mass of $10^{10} M_{\odot}$. The normalizations of GC (dashed) and M31 nucleus (dash-dotted) XLFs are arbitrary. The shaded areas around the curves show 1σ statistical uncertainty. Adapted from (Zhang et al., 2011).

5.2 Clues from luminosity functions

Variations in the shapes of the LMXB XLFs between field and GC environments have provided valuable insights into the nature and evolution of the LMXB population. Studies of the field and GC LMXB XLFs revealed that the shapes of the XLFs differ significantly, with the GC LMXB XLF appearing flatter than that of the field (Fig. 8, 9) (Zhang et al., 2011; Peacock et al., 2014; Peacock & Zepf, 2016). Furthermore, reports of an age dependence, in which the number of field LMXBs per galaxy stellar mass declines with increasing light-weighted stellar age (e.g., Kim & Fabbiano, 2010; Lehmer et al., 2014), suggested that the field LMXB XLF appeared to evolve with stellar age, a result expected from XRB population synthesis models (e.g., Fragos et al., 2009, 2013) and indirectly observed in deep *Chandra* surveys as an increase of the $L_X(\text{LMXB})/M_*$ scaling relation with increasing redshift (e.g., Lehmer et al., 2007, 2016; Aird, Coil, & Georgakakis, 2017). However, these studies suffered from small number statistics and large uncertainties on light-weighted stellar ages.

A more recent study by (Lehmer et al., 2020) culled 24 nearby early-type galaxies with *Chandra*, *Hubble*, and additional multiwavelength observations with the aim of investigating the nature of the field LMXB XLF. This work showed that early-type galaxies contain stellar-mass weighted ages that span only a narrow range where in-situ LMXB XLFs are not expected to vary. Global modeling of the field LMXB XLFs required scaling from both stellar mass and GC specific frequency with high confidence. Furthermore, the shape of the GC-related field LMXB XLF component was shown to be consistent with the XLF of LMXBs directly coincident with GCs, suggesting that some seeding of the field LMXB population from GCs is likely and significant in massive early-type galaxies. The right panel of Figure 9 shows the

level of contributions expected to the integrated $L_X[\text{LMXB}]/M_*$ as a function of S_N for in-situ LMXBs, GC seeded LMXB observed in galactic fields, and LMXBs directly coincident with GCs.

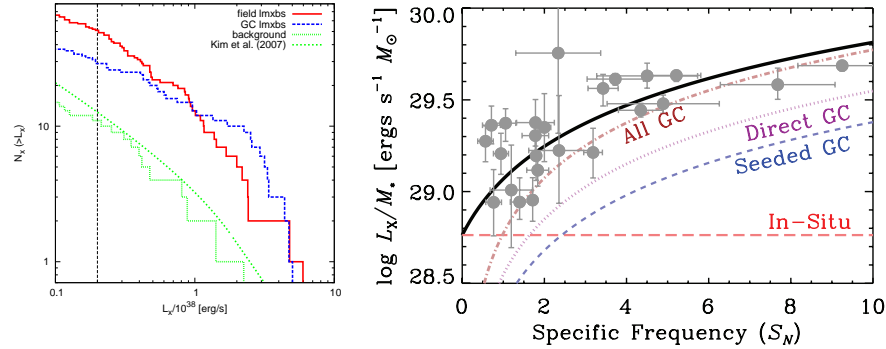


Fig. 9 (Left) Cumulative field (red solid) and GC (blue dashed) LMXB luminosity functions for NGC 4594 from (Peacock et al., 2014), illustrating the flatter XLF of GC LMXBs relative to field LMXBs. (Right) X-ray luminosity per stellar mass versus GC specific frequency, S_N , for a sample of 24 nearby elliptical galaxies (Lehmer et al., 2020). Contributions are shown for LMXBs that are formed “in situ” within the galactic fields (red long-dashed), those that are observed in galactic fields, but suspected of being formed in, and ejected from GCs (blue short-dashed), and those that are directly coincident with GCs (purple dotted).

5.3 Clues from the spatial distributions

Evidence supporting at least some contribution of GC seeding has also been observed in the spatial distributions of LMXBs in early-type galaxies. Zhang, Gilfanov, & Bogdán (2013) showed that the radial distributions of LMXBs in 20 early-type galaxies mainly followed the stellar light profiles, but contained an excess of low-luminosity ($\lesssim 5 \times 10^{38}$ ergs s^{-1}) X-ray sources out to ≈ 10 effective radii (Fig. 10). Such an excess is consistent with being associated with blue (metal poor) GCs, which follow broader profiles relative to stellar light, however it is also observed in galaxies with low GC content – the extended LMXB halos must be a combined result of GC seeding and neutron-star LMXBs being kicked out of the main bodies of their host galaxies by asymmetric supernova explosions (Zhang, Gilfanov, & Bogdán, 2013).

High stellar densities where stellar interactions become important are also reached in the galactic nuclei – similar to globular clusters they may become the site of the dynamical formation of LMXBs. Voss & Gilfanov (2007a,b) found a significant increase of the specific frequency of X-ray sources in the nucleus of M31 (Fig. 10). The large volume of the bulge and correspondingly large number of dynamically formed

LMXBs (about ~ 20 with $L_X > 10^{36}$ erg/s) permitted them to directly probe the density profile of dynamically formed binaries which was shown to follow ρ_*^2 law (Fig. 10, right bottom panel). As galactic bulges have $\sim 1 - 1.5$ orders of magnitude larger velocity dispersion than globular clusters, the details of stellar interactions and composition of dynamically formed binary populations are different in bulges and clusters (Voss & Gilfanov, 2007b).

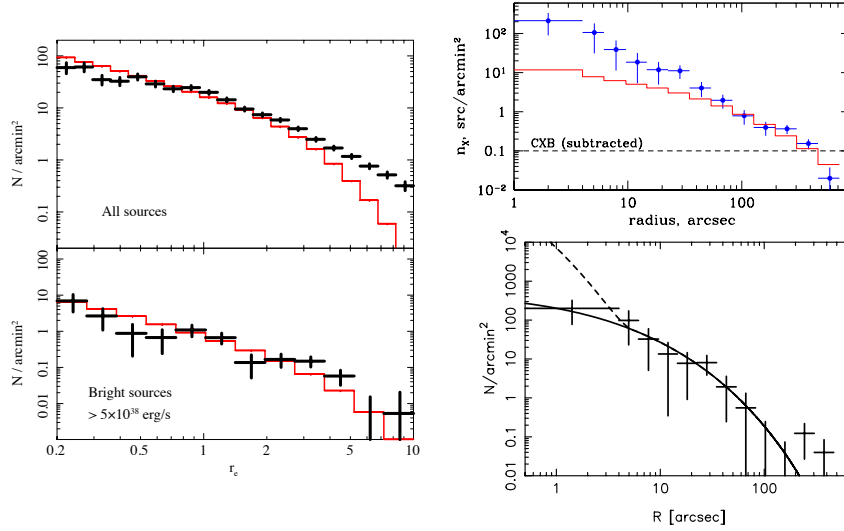


Fig. 10 *Left*: Stacked radial source density profiles of LMXBs in nearby early type galaxies, segregated by the source luminosity. Contribution of CXB removed. Solid histograms show predicted distribution based on the k_s -band light. The x-axis shows radial distance in units of the effective radius. Adapted from (Zhang, Gilfanov, & Bogdán, 2013). *Right*: Dynamical formation of LMXB in the nucleus of M31. The top panel shows radial distribution of LMXBs in the nucleus of M31, excluding globular cluster sources. The CXB level is subtracted (shown by the dashed line). The solid histogram shows the projected distribution of the stellar mass. The normalization of the latter is from the best fit to the data outside 1 arcmin. The bottom panel shows distribution of the “surplus” X-ray sources, computed as a difference between the data and the stellar mass model shown in the top panel. The solid line shows the projected ρ_*^2 distribution, computed from the same mass model of the M31 bulge. Adapted from (Voss & Gilfanov, 2007b)

Detailed investigations of the spatial distributions of GC populations in the elliptical galaxies NGC 4261, NGC 4649, and NGC 4278 show anisotropies that are consistent with anisotropies observed in the distributions of both GC and field LMXBs (Zezas et al., 2003; D’Abrusco et al., 2014; D’Abrusco, Fabbiano, & Brassington, 2014). The GC anisotropies show arc and streamer-like morphologies, indicative of past dwarf-galaxy mergers. The observed anisotropies in the field LMXB distributions could be due to GC LMXB ejection or could be relics of past star-formation in the merging systems.

A particularly good study case is that of NGC 4649, a giant E in the Virgo cluster. This study was made possible by the coordinated complete deep coverage of both

GC and LMXB populations with HST and Chandra surveys, which resulted in reliable identifications of X-ray sources with GC counterparts (Strader et al., 2012; Luo et al., 2013). Using these rich data sets, Mineo et al. (Mineo et al., 2014) concluded that the evolution of field binaries and the dynamical formation in GCs are both likely to occur: LMXBs spatially coincident with GCs follow the same radial distribution as the overall distributions of red and blue GCs, instead those with no GC counterpart are radially distributed like the stellar surface brightness, except perhaps at larger radii. Interestingly, in the 2-dimensional distributions of LMXBs and GCs on the plane of the sky in NGC 4649 there are arc-like distributions of GCs associated with similar over-densities of LMXBs (D’Abrusco et al., 2014; D’Abrusco, Fabbiano, & Brassington, 2014). However, a significant localized over-density of field LMXBs is found to the south of the GC arc, suggesting that these LMXBs may be somewhat connected with the arc of GCs. These sources occur at relatively large galactocentric radii and could contribute to the excess of field LMXB reported in Mineo et al. (2014).

6 Ultra-luminous X-ray sources.

An unusual class of compact sources – ultraluminous X-ray sources (ULXs), was discovered in the first survey of nearby galaxies with the Einstein Observatory in the late 1970s (see reviews (Fabbiano, 1989; Kaaret, Feng, & Roberts, 2017)). What characterizes these sources is their X-ray luminosity $L_X > 10^{39}$ erg/s, in excess of that expected from the Eddington limit for an object of 1-5 solar mass. This was at time the range of known masses for the compact accretor in Milky Way XRBs (neutron stars and stellar mass black holes). This discovery led to the speculation that ULXs could represent an entirely new class of astrophysical objects, Intermediate Mass Black Holes (IMBH), with masses $100 - 10^4$ solar mass, bridging the gap between the stellar black holes and the supermassive 10^8 solar mass black holes at the nuclei of galaxies (e.g. Colbert & Mushotzky, 1999).

However, a number of alternative models were advanced as well – from collimated radiation (Koeding, Falcke, Markoff, 2002) to \sim stellar mass black holes, representing the high mass tail of the standard stellar evolution sequence and accreting in the near- or slightly super-Eddington regime (King et al. , 2001; Grimm, Gilfanov, & Sunyaev, 2003; Gilfanov & Merloni, 2015). Also, a critical review of the observational properties of ULXs demonstrated that their association to IMBH, while possible, was not proven beyond reasonable doubt (Fabbiano, 2005).

As discussed below, Chandra observations have shown a prevalent (but not unique) association of ULXs with regions of intense star formation in galaxies, supporting the hypothesis of a stellar nature for these objects. Recent gravitational wave observations have also demonstrated that stellar BHs can have much higher masses than previously thought (up to 100 solar masses (Barrera & Bartos, 2022) ²). More

² see also <https://www.ligo.caltech.edu/image/ligo20171016a>

recently, the NuSTAR discovery of several pulsating ULXs (Bachetti et al., 2014; Walton et al., 2018), has changed dramatically the landscape of theoretical models, confirming the old theoretical prediction that the accretion column on the magnetic pole of a neutron star is less subject to the Eddington limit constrain (Basko & Sunyaev, 1975, 1976; King et al., 2001).

The present view on the nature of ULXs is more nuanced. It is quite possible that these luminous sources do not represent a unique astrophysical class of object. They may include super-Eddington XRBs (either NS or BH binaries), and also IMBH, especially in the case of very luminous ULXs at the outer radii of their associated galaxy (e.g. Kim et al., 2015).

6.1 Association with star-formation

The XLFs of compact X-ray sources in nearby early and late type galaxies (Fig. 5) make it quite obvious that luminous X-ray sources with $L_X \gtrsim 10^{39}$ erg/s are present in significant numbers only in star-forming galaxies where XLF extends into the range of luminosities attributed to ULXs, to $L_X \sim 10^{40}$ erg/s. Detailed studies of X-ray binary populations in individual galaxies showed that ULXs are preferentially located in or near star-forming regions (e.g. Colbert et al., 2004; Mineo et al., 2013; Zezas & Fabbiano, 2002; Zezas et al., 2007). Furthermore, comparison between the location of the ULXs and their nearest star-clusters or star-forming regions set stringent constraints on the strength of supernova kick velocities (Zezas & Fabbiano, 2002; Kaaret et al., 2004).

These results have been confirmed by more recent studies of ULXs in large samples of galaxies observed with *Chandra* Kowlakas et al. (2020); Swartz et al. (2011), which showed that ULXs are predominantly located within late-type galaxies with high sSFR. A particularly strong trend is the prevalence of ULXs in galaxies with low-metallicity (Mapelli, Colpi, & Zampieri, 2009; Brorby et al., 2016; Kowlakas et al., 2020; Prestwich et al., 2013). This trend is attributed to the weaker stellar winds of lower metallicity stars, resulting in tighter orbits and hence larger fraction of systems undergoing very efficient mass transfer (e.g. Linden et al., 2010; Fragos et al., 2013).

In contrast, searches for ULXs in early-type galaxies showed that they are rather scarce and are found predominantly in young ellipticals (Fig. 6). Zhang, Gilfanov and Bogdan (Zhang, Gilfanov & Bogdan, 2012) found 24 sources with $L_X > 10^{39}$ erg/s within D_{25} in a sample of 20 early type galaxies with measured stellar age, the expected number of background AGN being equal to 11.8. The luminous sources are mostly associated with younger galaxies – 17 and 7 in galaxies younger and older than 6 Gyrs, with the CXB sources expectation of 5.8 and 6 respectively. The specific frequencies of luminous sources are 8.8 ± 3.2 sources per $10^{12} M_\odot$ in young galaxies with the 90% upper limit of 2.9 sources per $10^{12} M_\odot$ in galaxies older than 6 Gyrs (Zhang, Gilfanov & Bogdan, 2012).

Similarly, Kouvakas and collaborators (Kouvakas et al., 2020) found a small number of ULXs in early-type galaxies which appears to correlate non-linearly with the stellar mass of their host galaxy. They interpreted this behaviour in the context of variations in the star-formation history of the galaxies, in agreement with ULX population synthesis models Kouvakas et al. (2020).

6.2 Main conclusions from optical studies

The association of ULXs with intensely star-forming galaxies provided the first indications that they are a sub-class of HMXBs. However, systematic studies of their environment showed that ULXs are often located inside bubbles of ionized gas as witnessed for strong He II, or O III lines (e.g. Kaaret & Corbel, 2009). While many of these bubbles are shock-excited by outflows from the ULX, the presence of strong excitation lines (e.g. He II, Ne V) in some of them clearly indicates photoionization by a hard ionizing source. In this case they can provide a direct measure of the soft X-ray luminosity of the ULX and therefore an stringent constraints on any beaming. The circular shape of many of these bubbles and the high inferred ionising luminosity (e.g. $> 10^{40} \text{ erg s}^{-1}$ in the case of HoII-X1 (Berghea et al., 2010)) suggests mild beaming.

Searches for optical counterparts to ULXs have been successful for ~ 20 sources Tao et al. (2011); Gladstone et al. (2013). These tend to have V-band luminosities similar to early-type star supergiants and blue colours. However, their optical SEDs are not consistent with stellar spectra, indicating that they are dominated by the accretion disk component Kaaret, Feng, & Roberts (2017).

6.3 Inferences from the shape of the HMXB luminosity function

As it has been well known, the maximum mass of a black holes produced in the course of standard stellar evolution at solar abundance of elements is limited to $\approx 10 - 20 M_{\odot}$, whereas formation of more massive black holes with mass exceeding ~ 100 is only possible at virtually zero abundance of metals (Zhang, Woosley & Heger, 2008). It is not quite clear yet, whether this conventional picture contradicts the LIGO detections of $\sim 100 M_{\odot}$ black holes in coalescing binaries (Barrera & Bartos, 2022). It is possible in principle that the most luminous sources are accreting IMBHs – descendants of Pop III stars, which acquired a massive companion in star-forming regions. Obviously, the abundance of such systems should be significantly smaller than abundance of normal high-mass X-ray binaries formed in the course of standard stellar evolution. Therefore there must be a break in the luminosity function at the transition between "normal" X-ray binaries and these objects. However, observations show that the luminosity distribution of compact X-ray sources in star forming galaxies smoothly extends up to the luminosities of

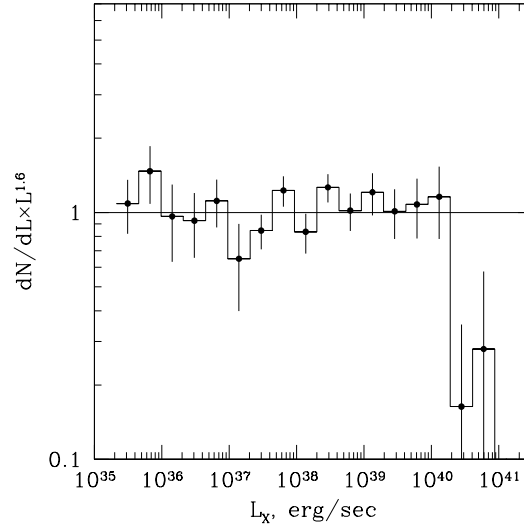


Fig. 11 Detailed shape of the X-ray luminosity function of compact X-ray sources in star-forming galaxies. The figure shows the ratio of the X-ray luminosity function from Fig. 5 to a power law with slope of 1.6. Based on results of Mineo, Gilfanov & Sunyaev (2012).

$\log L_X \sim 40 - 40.5$, without any significant features or slope changes. In particular, unlike the LMXB LXF, it does not have any significant features at the luminosities corresponding to the Eddington limit of a neutron star ($\log L_X \sim 38.3$) or of a black hole ($\log L_X \sim 39 - 39.5$). On the other hand, it breaks at the luminosity $\log L_X \approx 40.0 - 40.5$ (Fig. 11), corresponding to the Eddington luminosity of a $\sim 100 M_\odot$ object. Because of such a smooth shape of their XLF, it appears most likely that systems with luminosity $\log L_X \leq 40 - 40.5$ are “normal” X-ray binaries formed in the course of standard stellar evolution and represent the tail of the distribution of black hole masses and mass accretion rates. We note here that luminosities exceeding the Eddington limit by several times are possible in the standard accretion model (Shakura & Sunyaev, 1973; Grimm, Gilfanov, & Sunyaev, 2003). The break in the HMXB XLF observed at $\log L_X \sim 40.5$ (Fig. 5, 11) may indicate the transition to a different population of X-ray sources. The few known sources with luminosities exceeding this value may indeed be IMBHs – result of the evolution of Pop III stars.

6.4 Possible nature and implications for accretion physics

The nature of ULXs has been a matter of debate since their discovery in the early 1980s, with potential models including super-luminous supernova remnants, accreting IMBHs, highly accreting X-ray binaries formed through dynamical capture or secular evolution (see e.g. Zezas & Fabbiano, 2002; Fabbiano, 2006; Kaaret, Feng,

& Roberts, 2017, for a critical summary of these models). Mounting evidence based on their X-ray luminosity distribution, association with young stellar populations, scaling with SFR and metallicity, and their multi-wavelength counterparts or surrounding nebulae, suggests that the vast majority of ULXs are HMXBs undergoing a rapid mass-transfer episode. In this respect they are the upper end of the X-ray luminosity range of HMXBs. In fact, detailed modeling of the mass-transfer sequences of HMXBs (e.g. Rappaport, Podsiadlowski, & Pfahl, 2005) indicates that systems with massive donors ($\gtrsim 10M_{\odot}$) can undergo brief phases ($\sim 10^2 - 10^4$ yr) of mildly super-Eddington accretion resulting in X-ray luminosities even in excess of $\sim 10^{40}$ ergs s^{-1} . These episodes take place at the thermal-timescale of the donor star. These results are supported by a growing volume of X-ray binary population-synthesis models which show that indeed HMXBs can experience brief phases of super-Eddington mass transfer which in some cases can reach accretion rates well in excess of $10^3 \dot{M}_{\text{Edd}}$; the fraction of these super-Eddington systems increases dramatically in lower metallicities (e.g. Linden et al., 2010; Wiktorowicz et al., 2017; Marchant et al., 2017).

Further evidence for supercritical accretion comes from the discovery of pulsar-ULXs which gives a direct constraint on the compact object mass (e.g. Bachetti et al., 2014). A natural outcome of supercritical accretion is the formation of the so-called slim or thick accretion disks. The slim disks are expected to form at accretion rates exceeding $\sim \dot{M}_{\text{Edd}}$, and they have larger height (thickness) than the standard thin disks (Shakura & Sunyaev, 1973; Szuszkiewicz, Malkan, & Abramowicz, 1996), resulting in non-linear scaling of the emerging X-ray luminosity with accretion rate and different spectral shape. In higher accretion rates the radiation pressure further increases its thickness resulting in the formation of a funnel in its inner part (Szuszkiewicz, Malkan, & Abramowicz, 1996). A natural outcome of this effect is mild beaming of the X-ray emission (e.g. King, 2002). Recent general relativistic, radiation magneto-hydrodynamical simulations of supercritical mass accretion models for black holes confirmed this picture (e.g. Sadowski & Narayan, 2016).

The differences in the structure of the accretion disk in ULXs with respect to lower-luminosity X-ray binaries becomes evident in their X-ray spectra, which often show a curvature above ~ 2 keV which can be described by a break at $\sim 7 - 10$ keV (Poutanen et al., 2007; Kaaret, Feng, & Roberts, 2017, and references therein). Evidence of reflection of the pulsar emission from the walls of the accretion funnel has been also found (Bykov et al., 2022).

7 Population synthesis results

7.1 *Relevant results from binary evolution*

X-ray binary evolution models have provided important insights in the formation timescales of the different types of X-ray binaries. These are determined by a com-

bination of the nuclear timescales of the donor stars and the time required for the onset of mass transfer from the donor star to the compact object. The mass transfer can take place in two main ways: (a) capture of material expelled from the donor star in the form of a stellar wind, and (b) Roche-lobe overflow. The stellar winds are mostly relevant in the case of X-ray binaries with early-type donors (O,B stars, supergiants, or Wolf-Rayett stars), since lower-mass stars have very weak stellar winds that cannot produce observable X-ray emission. A special case of wind-fed X-ray binaries are the Be X-ray binaries (Be-XRBs) where the accreted material originates in an equatorial outflow (decretion disk) from the donor Oe or Be star (e.g. Reig, 2011). On the other hand, the onset of Roche-lobe overflow (RLOF) requires that the radius of the donor star becomes larger than its Roche lobe. This usually happens either as a result of the increase of the stellar radius as the star evolves off the main sequence, and/or as a result of the shrinkage of the orbital radius of the system (e.g. due to tidal evolution, magnetic breaking, common-envelope evolution etc).

Since the donor stars have lower mass than the primary star producing the compact objects, their nuclear evolution timescales are longer. High-mass X-ray binaries appear between a few Myr and ~ 100 Myr from the formation of the binary stellar system. The low limit is driven by the time required for the most massive star of the system to produce a compact object. The upper range reflects the upper range of the timescale needed for the donor star (which in the case of HMXBs is of O or B spectral types) to evolve and initiate the mass transfer. In the case of Low Mass X-ray binaries, their formation timescales are much longer, from a few hundred Myr up to several Gyr. This is because because of the longer evolutionary timescales of lower-mass donor stars, and the long timescale required for the shrinkage of the orbital radius.

Binary stars are formed with a wide range of mass ratios, orbital separations, and eccentricity. Only a small fraction of these systems will eventually become X-ray binaries (Section 7.3). Even before the formation of a compact object as a result of the nuclear evolution of the more massive star, the two stars may interact, exchanging mass. The supernova explosion may have a dramatic effect in the evolution of the system by imparting a kick onto the resulting compact object. The result of the kick is to increase the orbital separation and/or the eccentricity of the orbit. In the most extreme case it may disrupt the binary system. However, as a result of the nuclear evolution of the secondary, mass transfer either through a stellar wind or RLOF may initiate, resulting in an X-ray binary. If the mass of the donor star is lower than $\sim 10M_{\odot}$ the initiation of mass transfer also requires shrinkage of the orbit. This can take place through a variety of mechanisms: magnetic breaking, tidal interaction, emission of gravitational radiation. A particularly effective mechanism is common envelope evolution (e.g. Taam & Sandquist, 2000; Ivanova, Justham, & Ricker, 2020), which however, in many cases may lead to the merging of the two systems.

7.2 Summary of population synthesis models and their results

X-ray binary population synthesis models are an invaluable tool for understanding the X-ray binary populations, their connection with fundamental parameters of the host galaxy and for constraining uncertain parameters of the theory through comparisons with observations. They calculate the populations of X-ray binaries at a given time of the evolution of a stellar population by combining distributions of the initial parameters of the binary systems together with prescriptions for the evolution of the stars in the binary systems and its orbital parameters (e.g. Belczynski et al., 2008; Riley et al., 2022; Fragos et al., 2013). As a result, one then can model the X-ray emission of different X-ray binary populations as a function of the star-formation history of their parent stellar populations.

Figure 4 shows the dependence of the integrated X-ray luminosity of a stellar population as a function of its age and metallicity. It is clear that X-ray binary populations associated with younger and lower metallicity stellar populations tend to have higher X-ray luminosities. The metallicity dependence is particularly important for understanding the cosmological evolution of X-ray binary populations and their potential role in the early Universe (Section 8).

The first attempts to model the X-ray binary populations observed with *Chandra* using population synthesis showed that despite the large number of parameters in these models, their results are relatively robust (e.g. Belczynski et al., 2008; Riley et al., 2022; Fragos et al., 2013). Nonetheless, comparison of the X-ray luminosity functions of X-ray binaries obtained in *Chandra* led to useful constraints on parameters such as the strength of the stellar winds, the common-envelope ejection efficiency, and the mass-ratio of the stars in the binary system at the zero-age main sequence Tzanavaris et al. (2013). Similar constraints can be set by looking at the integrated X-ray emission of X-ray binaries in unresolved galaxies (e.g. Fragos et al., 2013; Lehmer et al., 2016). Furthermore, comparison of the measured age-evolution of the formation rate of X-ray binaries with predictions from X-ray binary population synthesis models showed (Fig. 3) that they reproduce well the increased populations at ages $\sim 10 - 50$ Myr and the decline of their integrated X-ray luminosities at systems older than ~ 5 Gyr, as well as, their metallicity dependence (Shtykovskiy & Gilfanov, 2007; Antoniou et al., 2010; Antoniou & Zezas, 2016; Antoniou et al., 2019; Lehmer et al., 2021).

In the case of ULXs, population synthesis models showed that their increased rates at low metallicities is driven by the reduced effect of stellar winds in removing mass and angular momentum from the system and hence resulting in tighter orbits and a larger fraction of systems undergoing RLOF mass transfer (e.g. Linden et al., 2010). Furthermore, detailed modeling of individual ULXs (and especially pulsar-ULXs) revealed additional formation channels for these rare but very luminous systems (e.g. Misra et al., 2020; Abdusalam et al., 2020).

7.3 How frequent are X-ray binaries?

With the knowledge of the relation between the number of HMXBs and SFR, we can estimate the fraction of compact objects that become HMXBs (Mineo, Gilfanov & Sunyaev, 2012). According to the HMXB XLF and scaling relation (Section 3), the number of HMXBs with luminosity higher than 10^{35} erg/s is:

$$N_{\text{HMXB}}(> 10^{35} \text{ erg s}^{-1}) \approx 135 \times \text{SFR} \quad (8)$$

On the other hand, the number of HMXBs can be expressed via the birth rate of compact objects \dot{N}_{co} :

$$N_{\text{HMXB}} \sim \dot{N}_{co} \sum_k f_{X,k} \tau_{X,k} \sim \dot{N}_{co} f_X \bar{\tau}_X \quad (9)$$

The \dot{N}_{co} approximately equals to the birth rate of massive stars $\dot{N}_*(M > 8M_\odot) \approx 7.4 \cdot 10^{-3} \times \text{SFR}$.³ The $f_X = \sum_k f_{X,k}$ is the fraction of compact objects which become X-ray active in HMXBs and $\bar{\tau}_X$ is the average X-ray life time of such objects. As discussed in Mineo, Gilfanov & Sunyaev (2012), the low and moderate luminosity sources are dominated by Be/X systems, therefore $\bar{\tau}_X \sim 0.1$ Myr (cf. Fig. 3) (Verbunt & van den Heuvel, 1995). Combining equations 8 and 9, we obtain:

$$f_X \sim 0.18 \times \left(\frac{\bar{\tau}_X}{0.1 \text{ Myr}} \right)^{-1} \quad (10)$$

Thus, we arrived to a remarkable conclusion that a large fraction, of the order of \gtrsim ten per cent of all black holes and neutron stars once in their lifetime were X-ray sources with $L_X > 10^{35}$ erg/s, powered by accretion from a massive donor star in a high-mass X-ray binary.

Similarly, given the scaling relation for ULXs $N_{\text{ULX}}(> 10^{39} \text{ erg/s}) \approx 0.48 \times \text{SFR}$ one can show that

$$f_{\text{ULX}} \sim 3.5 \cdot 10^{-2} \times \left(\frac{\bar{\tau}_{\text{ULX}}}{10^4 \text{ yr}} \right)^{-1} \quad (11)$$

i.e. a few per cent of all black holes formed in a galaxy become ultra-luminous X-ray sources with luminosity $\geq 10^{39}$ erg/s, explaining the observed population of ULXs.

Interestingly, only $f_{\text{LMXB}} \sim 10^{-6}$ of compact objects become X-ray bright in LMXBs (Mineo, Gilfanov & Sunyaev, 2012). This is another manifestation of the fact that LMXBs are extremely rare objects and may be explained by the high probability of disruption of the binary system with a low mass companion in the course of the supernova explosion.

These numbers provide valuable input for calibration of the population synthesis models.

³ use of the Salpeter IMF is explained in Mineo, Gilfanov & Sunyaev (2012)

7.4 Connection to LIGO-Virgo sources

X-ray binaries are one of the few easily observable phases in the evolution of binary stellar systems. Furthermore, since the onset of mass transfer requires small orbital separation, a fraction of X-ray binaries is expected to become binary compact object systems which will merge within a Hubble time producing gravitational-wave sources (e.g. Marchant et al., 2017). Therefore, the study of X-ray binaries is inextricably linked to the study of the gravitational-wave sources: X-ray binaries provide information on the demographics of the compact object populations (e.g. Farr et al., 2016) and constraints on X-ray binary formation and evolution models. Furthermore, joint study of the compact object populations inferred from gravitational-wave observations and X-ray binaries will provide a more complete picture of their overall mass spectrum and spin distribution (e.g. Fishbach & Kalogera, 2022).

8 Cosmic evolution of X-ray binaries and their contribution to CXB

8.1 Contribution of X-ray binaries to cosmic X-ray background

Knowing how stellar mass was built in the Universe, a natural question to ask is how much X-ray binaries contribute to cosmic X-ray background (CXB). In order to answer this question, Dijkstra et al. (2012) combined the local $L_X - \text{SFR}$ and $L_X - M_*$ relations with the cosmic star-formation history. They found that star-forming galaxies contribute $\sim 5 - 15$ per cent to soft ($1 - 2$ keV) CXB and $\sim 1 - 20$ per cent to the hard band ($2 - 10$ keV) CXB. The main source of uncertainty in these estimate was associated with the uncertainty in the spectra of ULXs for which Dijkstra et al. (2012) allowed a conservatively broad range of photon index values $\Gamma = 1 - 3$. Assuming a more narrow interval of $\Gamma = 1.7 - 2.0$, contribution of star-forming galaxies to the soft CXB can be limited to $\approx 8 - 13$ per cent. The contribution to the CXB in the hard band is uncertain mostly because of a more uncertain K-correction at the corresponding high energies. For the parameters of the Chandra Deep Field North, they found that galaxies whose individual observed flux is below the detection threshold in the Chandra Deep Field North (CDF-N), can fully account for the unresolved part of the CXB in the soft band. This conclusion is insensitive to details in the model as long as the photon index, averaged over the entire population of X-ray-emitting star-forming galaxies, is $\Gamma < 2$, which corresponds to a very reasonable range given the existing observational constraints on Γ .

The tightness of remaining unresolved CXB permits one to constrain the evolution of the $L_X - \text{SFR}$ relation with redshift. When it is parameterised as $L_X/\text{SFR} = A(1+z)^b$, the unresolved soft CXB requires that $b < 1.6$ (3σ) (Dijkstra et al., 2012).

Due to much lower formation efficiency (Section 7.3), the contribution to CXB of LMXBs is at least an order of magnitude smaller (Dijkstra et al., 2012).

8.2 X-ray investigations of cosmologically distant galaxies

With the advent of deep extragalactic X-ray surveys (see, e.g., review by Brandt & Alexander, 2015), it is now possible to place meaningful observational constraints on the cosmic evolution of X-ray binary populations. The first deep (≈ 1 Ms depth) *Chandra* surveys in the *Chandra* Deep Field-North (CDF-N; Hornschemeier et al., 2000; Brandt et al., 2001) and CDF-South (CDF-S; Giacconi et al., 2001) revealed substantial numbers of “normal” galaxies at $z \lesssim 1.5$ with X-ray-to-optical flux ratios that were consistent with being powered primarily by XRBs and hot gas, without substantial contributions from active galactic nuclei (AGN). These discoveries gave way to the new and active field of X-ray studies of normal galaxies at cosmologically significant distances. Due to the dominance of XRB emission in normal galaxies at rest-frame wavelengths $> 1\text{--}2$ keV, combined with the redshifting of rest-frame soft emission out of the *Chandra* observed frame, X-ray emission detected in these distant normal galaxies is expected to primarily trace XRB populations. As the *Chandra* Deep Fields (CDFs) and additional survey fields accumulated X-ray depth and multiwavelength data, the insights on the cosmic evolution of XRB populations in galaxies expanded.

Studies of X-ray detected normal-galaxy samples in the CDFs have revealed that the galaxy XLF undergoes positive redshift evolution from the local universe to $z \approx 1.5$ (e.g., Ptak et al., 2007; Tzanavaris & Georgantopoulos, 2008). The evolution is primarily driven by late-type galaxy populations, which show luminosity evolution of the XLF at the $(1+z)^{0.4\text{--}3.4}$ level. The XLFs of early-type galaxies may also evolve with redshift, however, the relatively small numbers of early-type galaxies detected in the CDFs yield weak constraints on XLF evolution. The overall normal galaxy XLF evolution is primarily driven by the rising cosmic star-formation rate density from $z = 0\text{--}1.5$ (see, e.g., Madau & Dickinson, 2014, for a review), and scaling-relation investigations show that the X-ray detected galaxy population follows the local L_X/SFR correlation within the relations scatter (e.g., Mineo et al., 2014). However, thus far, X-ray detected normal galaxies in deep surveys number in the hundreds of objects, which represent only a small fraction (as low as 1% for *Hubble*-detected sources) of the galaxy population that is known to be present in these fields. As such, X-ray detected normal-galaxy population studies suffer from significant selection biases.

To investigate X-ray emission from more representative populations of galaxies, and scaling relations between X-ray binary population luminosity and galaxy properties, X-ray stacking of optically-selected galaxies has often been employed. Early stacking efforts initially showed that X-ray properties of normal galaxies were nearly consistent with basic local scaling relations (e.g., L_X/SFR and L_X/M_*) out to $z \approx 3$ once corrections for optical extinction and L_{opt} to SFR were accounted for (Hornschemeier et al., 2002; Basu-Zych et al., 2013; Symeonidis et al., 2014). However, as multiwavelength data sets expanded and *Chandra* depths and coverage increased, significant positive redshift evolution was detected in the HMXB and LMXB luminosity scalings with SFR and M_* , respectively, out to $z \approx 2.5$ (i.e., to a cosmic lookback time of ≈ 11 Gyr). The redshift evolution of these scal-

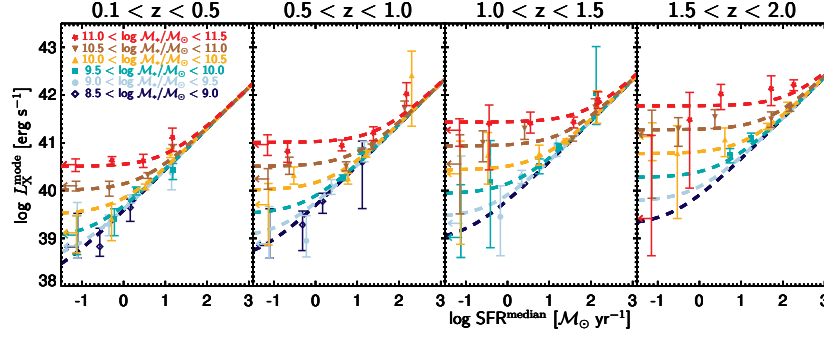


Fig. 12 Most probable X-ray luminosity for galaxy samples selected in bins of redshift, SFR, and M_* , based on analysis of samples in the CANDELS survey fields (Fig 7 of Aird, Coil, & Georgakakis, 2017). These data show a rise in L_X with redshift, after controlling for SFR and M_* , illustrating the positive evolution of X-ray emission from HMXBs ($L_X(\text{HMXB})/\text{SFR}$) and LMXBs ($L_X(\text{LMXB})/M_*$) with increasing redshift.

ing relations has been found to roughly follow $L_X(\text{HMXB})/\text{SFR} \propto (1+z)$ and $L_X(\text{LMXB})/M_* \propto (1+z)^{2-3}$ (e.g., Lehmer et al., 2016; Aird, Coil, & Georgakakis, 2017; Fornasini, Civano, & Suh, 2020), in good consistency with the CXB based constraints Dijkstra et al. (2012). Figure 12 illustrates constraints from Aird, Coil, & Georgakakis (2017), which show that the X-ray luminosity of typical galaxies rises with increasing redshift for fixed stellar mass and SFR.

8.3 Drivers of the Redshift Evolution of X-ray Binary Populations

The combination of detailed XRB population synthesis models and cosmological models of evolving galaxy populations provided a framework to construct models of the evolution of X-ray emission from XRBs and their scaling relations with physical properties. Fragos et al. (2013) used *Startrack* XRB population synthesis models (Belczynski et al., 2008) and simulated galaxy models from the Millenium II simulation (Guo et al., 2011) to track the XRB emission throughout the Universe from $z \approx 20$ to the present day. These models accounted for evolution in star-formation activity, stellar masses, stellar ages, and metallicities and identified best models that simultaneously reproduced local (i.e., $z = 0$) $L_X(\text{HMXB})/\text{SFR}$ and $L_X(\text{LMXB})/M_*$ scaling relations. As a byproduct, these models provided predictions for the redshift evolution of the scaling relations and the cosmic X-ray emissivity from XRB populations.

The predicted scaling relation evolution from the best Fragos et al. models was found to be similar to that observed empirically in the CDFs, and the models provided physical insight for the drivers of this evolution. The rise of $L_X(\text{HMXB})/\text{SFR}$ with redshift was expected to be driven by a corresponding decline in metallicity.

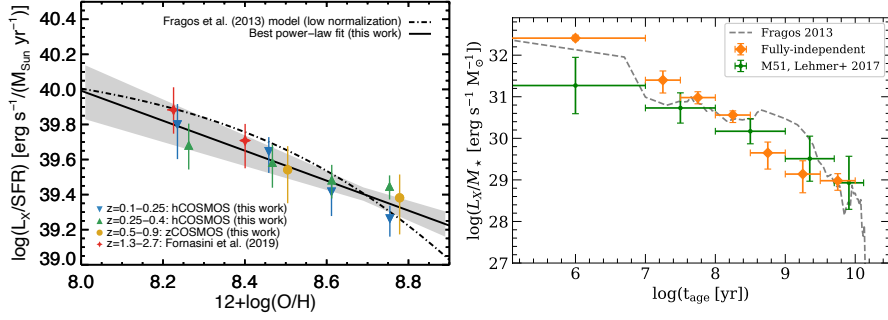


Fig. 13 (*Left*) The X-ray luminosity per SFR (L_X/SFR) versus gas-phase metallicity ($12 + \log(\text{O}/\text{H})$) for stacked samples of high specific star-formation rate galaxies at $z \approx 0.1-2.6$ in the CDF and COSMOS survey fields. The X-ray emission for these galaxies is expected to be dominated by young populations of HMXBs, and a clear anticorrelation is observed (black curve indicates best-fit relation), consistent with theoretical models (the dot-dashed curve from Fragos et al. (2013)). Adapted from Fornasini, Civano, & Suh (2020). (*Right*) Average age-dependence of the 2–10 keV luminosity per stellar mass (L_X/M_*) for 344 galaxies in the CDFs. A decline of ≈ 3 orders of magnitude is observed from 10 Myr to 10 Gyr as XRB populations become less luminous and powered by accretion from increasingly lower mass stars. Figure modified from its original version in (Gilbertson et al., 2021).

Stellar wind mass loss is expected to increase with metal content, and in the context of XRBs, relatively low metallicity systems are expected to lose less mass and angular momentum from stellar winds, allowing the binary orbits to remain relatively tight and yield larger mass-transfer rates and higher X-ray luminosities than relatively high metallicity systems. For LMXBs, the increase of $L_X(\text{LMXB})/M_*$ with increasing redshift was predicted theoretically as a result of the LMXB donor stars shifting to higher mass objects and higher mass-transfer rates as the ages of the stellar populations decline with increasing redshift.

8.4 Recent Constraints on X-ray Evolution of Galaxies

While theoretical models suggest that both metallicity and stellar age evolution are responsible for the observed evolution of XRB scaling relations, more direct empirical evidence has only recently supported these suggestions. For example, (Fornasini et al., 2019; Fornasini, Civano, & Suh, 2020) investigated HMXB-dominant galaxies (high SFR/M_*) at $z \approx 0.1-2.6$, located in the COSMOS and CDF-S fields, that had gas-phase metallicity measurements via strong emission-line indicators. They divided their galaxy samples into bins of redshift and gas-phase metallicity and used X-ray stacking to show that the mean $L_X(\text{HMXB})/SFR$ ratio declined with increasing metallicity in a single relation that is consistent with local-galaxy $L_X(\text{HMXB})/SFR-Z$ relations (e.g., Brorby et al., 2016; Lehmer et al., 2021) – see left-panel of Figure 13. To investigate age evolution of XRB populations, (Gilbertson et al.,

2021) measured star-formation histories of galaxies in the CDFs, and used a statistical method to construct a model of L_X/M_* versus age consistent with the galaxy X-ray counts. A decline of three orders of magnitude was observed for L_X/M_* from ≈ 10 Myr to ≈ 10 Gyr, mainly consistent with expectations from the Fragos et al. (2013) models (right-panel of Figure 13).

8.5 Contribution to (pre)heating of IGM

The large mean-free path of X-ray photons suggests that they can penetrate a larger volume of the interstellar medium around the X-ray source. This becomes particularly important in the early Universe ($z > 10$), where they may influence a larger volume around the primordial galaxies than the ultraviolet photons associated with the first Population-III stars (e.g. Madau & Fragos, 2017, and references therein). This results in heating of the primordial intergalactic medium even before the epoch of reionization, which has important implications for the subsequent galaxy formation (e.g. Artale, Tissera, & Pellizza, 2015).

Extrapolation of the best XRB population synthesis models to $z \approx 3$ –20, where only weak empirical constraints are currently available, indicate that X-ray emissivity of the Universe from HMXBs is likely to exceed AGN at $z \gtrsim 6$ –8 (e.g., Fragos et al., 2013; Madau & Fragos, 2017). At these redshifts, $L_X(\text{HMXB})/\text{SFR}$ is expected to be elevated over the local relation by a factor of ~ 10 due to differences in metallicity. As an added result, the escaping radiation at low energies $\lesssim 2$ keV may be further enhanced due to the lack of metal absorption edges that significantly impact the optical depth at these energies (e.g., Das et al., 2017). As a consequence of these effects, HMXB populations are of particular interest as having a potentially significant role in heating of the intergalactic medium at $z \gtrsim 10$. The impact of this heating is expected to be imprinted at these redshifts on the cosmic 21-cm brightness temperature relative to the cosmic microwave background, and numerous efforts are underway to directly observe these signatures. For example, the Hydrogen Epoch of Reionization Array (HERA; e.g., DeBoer et al., 2017) and Square Kilometre Array (SKA; e.g., Mellema et al., 2013), are predicted to directly constrain the 21-cm signal over a wider range of redshift and will enable constraints on $L_X(\text{HMXB})/\text{SFR}$ associated with the galaxy populations there (see, e.g., The HERA Collaboration et al., 2021, for first results).

9 Concluding remarks

Sub-arcsecond angular resolution of Chandra observatory led to a quantum leap in our understanding of populations of X-ray binaries in external galaxies, their content, evolution and scaling with fundamental parameters of galaxies. In over 20 years of operation in space, Chandra observed hundreds of galaxies of various morpho-

logical types, ages and metallicities. X-ray luminosity functions of compact sources in young and old galaxies to the meaningful depth have been obtained for many dozens of galaxies, providing the ultimate proof of their nature as high- and low-mass X-ray binaries. Their spatial distributions have been obtained and compared with the distributions of various tracers, confirming that different formation channels are in place, primordial and dynamical. These observations provided wealth of information for calibration and verification of population synthesis models which in turn gave valuable feedback to the theories of stellar and binary evolution. Deep Chandra fields permitted to study collective properties of high-mass X-ray binaries in distant galaxies, located at cosmological redshifts, to study their evolution and to make further comparisons with binary population modelling. These studies revealed an unanticipated role of star-forming galaxies and their X-ray binaries in preheating the inter-galactic medium in early Universe and in shaping the Cosmic X-ray background, and also led to the proposition of a new independent method to measure star-formation rate in (distant) galaxies.

Along with these remarkable advances, many unanswered questions still remain. The list of outstanding goals for future studies includes, to mention a few: the redshift evolution of X-ray binaries, the nature and formation channels of ultra-luminous X-ray sources and their connection to LIGO-Virgo sources, the maximum mass of "stellar mass" black holes and role of the intermediate mass ones, detailed understanding of dynamical formation of LMXBs in globular clusters and galactic nuclei and their metallicity dependence and seeding of field populations, the origin of the HMXB XLF, which maintains same slope over five orders of magnitude in luminosity, with only moderate deviations from the power law. On the other end of the luminosity range are fainter sources such as cataclysmic variables which extra-galactic populations are yet to be explored. There are still many complexities in the data which we do not quite understand, but existence of many others is yet to be recognised.

The progress of observational capabilities of modern astronomy, anticipated in the coming years and planned for the more distant future, will help to answer these questions and will inevitably raise the new ones. Eagerly awaited are the results from the SRG all-sky survey which is more than a half a way through. Its eROSITA telescope, although lacking the angular resolution of Chandra, will survey the entire sky eight times. It will detect of the order of $\sim 10^4$ normal galaxies of all morphological types, fully sampling the parameter space of normal galaxies. Critical role in many studies is played by observations at other wavelength, in particular, optical and infra-red. These will be advanced with the start of operations of the Vera C. Rubin Observatory and Euclid satellite. Smaller samples of carefully selected galaxies will be observed by the James Webb Space telescope. At the X-ray wavelengths, the major new thrust will be given by Athena and Lynx X-ray observatories. Notably, the Lynx Observatory will deliver the angular resolution of Chandra but at ~ 50 times higher throughput.

References

- Abdusalam K., Ablimit I., Hashim P., Lü G.-L., Mardini M. K., Wang Z.-J., 2020, *ApJ*, 902, 125
- Artale M. C., Tissera P. B., Pellizza L. J., 2015, *MNRAS*, 448, 3071
- Aird J., Coil A. L., Georgakakis A., 2017, *MNRAS*, 465, 3390
- Antoniou V., Zezas A., Hatzidimitriou D., Kalogera V., 2010, *ApJL*, 716, L140
- Antoniou V., Zezas A., 2016, *MNRAS*, 459, 528
- Antoniou V., Zezas A., Drake J. J., et al., 2019, *ApJ*, 887, 20
- Bachetti, M. et al. 2014, *Nature*, 514, 202
- Barrera O., Bartos I., 2022, *ApJL*, 929, L1
- Basko M. M., Sunyaev R. A., 1976, *MNRAS*, 175, 395
- Basko M. M., Sunyaev R. A., 1975, *A&A*, 42, 311
- Basu-Zych A. R., Lehmer B. D., Hornschemeier A. E., et al., 2013, *ApJ*, 762, 45
- Basu-Zych A. R., Hornschemeier A. E., Haberl F., et al., 2020, *MNRAS*, 498, 1651
- Belczynski K., Kalogera V., Rasio F. A., et al., 2008, *ApJS*, 174, 223
- Berghea C. T., Dudik R. P., Weaver K. A., Kallman T. R., 2010, *ApJ*, 708, 354
- Boroson B., Kim D.-W., Fabbiano G., 2011, *ApJ*, 729, 12
- Brorby M., Kaaret P., Prestwich A., Mirabel I. F., 2016, *MNRAS*, 457, 4081
- Brandt W. N., Alexander D. M., Hornschemeier A. E., et al., 2001, *AJ*, 122, 2810
- Brandt W. N., Alexander D. M., 2015, *A&ARv*, 23, 1
- Bykov S. D., Gilfanov M. R., Tsygankov S. S., Filippova E. V., 2022, *MNRAS*, 516, 1601
- Cheng Z., Li Z., Xu X., Li X., 2018, *ApJ*, 858, 33
- Clark, D. H., & Parkinson, J. H. 1975, *Nature*, 258, 408
- Colbert E. J. M. & Mushotzky R. F., *ApJ*, 519, 89 (1999)
- Colbert E. J. M. et al. *ApJ*, 602, 231 (2004)
- D'Abrusco R., Fabbiano G., Mineo S., et al., 2014, *ApJ*, 783, 18
- D'Abrusco R., Fabbiano G., Brassington N. J., 2014, *ApJ*, 783, 19
- David L. P., Jones C., Forman W., 1992, *ApJ*, 388, 82
- Dage K. C., Zepf S. E., Peacock M. B., et al., 2019, *MNRAS*, 485, 1694
- Das A., Mesinger A., Pallottini A., Ferrara A., Wise J. H., 2017, *MNRAS*, 469, 1166
- DeBoer D. R., Parsons A. R., Aguirre J. E., et al., 2017, *PASP*, 129, 045001
- Dijkstra M., Gilfanov M., Loeb A., Sunyaev R., 2012, *MNRAS*, 421, 213
- Fabbiano, G. 1988, *ApJ*, 325, 544
- Fabbiano, G., Kim, D.-W., Trinchieri, G. 1992, *ApJS*, 80, 531
- Fabbiano G., *ARA&A*, 27, 87 (1989)
- Fabbiano G., Zezas A., Murray S. S., 2001, *ApJ*, 554, 1035
- Fabbiano, G., & Shapley, A. 2002, *ApJ*, 565, 908
- Fabbiano, G. 2005, *Science*, Vol. 307, p. 533-534
- Fabbiano G., *ARA&A*, 44, 323 (2006)
- Fabbiano, G. 2019, in *The Chandra X-ray Observatory*, by Wilkes, Belinda; Tucker, Wallace. ISBN: 978-0-7503-2163-1. IOP ebooks. Bristol, UK: IOP Publishing, 2019, pp. 7-1-7-42
- Fabian, A. C., Pringle, J. E., & Rees, M. J. 1975, *MNRAS*, 172, 15P
- Farr B., Berry C. P. L., Farr W. M., et al., 2016, *ApJ*, 825, 116
- Fishbach M., Kalogera V., 2022, *ApJL*, 929, L26
- Fornasini F. M., Kriek M., Sanders R. L., et al., 2019, *ApJ*, 885, 65
- Fornasini F. M., Civano F., Suh H., 2020, *MNRAS*, 495, 771
- Fragos T., Kalogera V., Willems B., et al., 2009, *ApJL*, 702, L143
- Fragos T., Lehmer B., Tremmel M., et al., 2013, *ApJ*, 764, 41
- Galiullin I., Gilfanov M., Sunyaev R., 2023, *MNRAS*, in preparation
- Garofali K., et al., 2018, *MNRAS*, 479, 3526. doi:10.1093/mnras/sty1612
- Ghosh P., White N. E., 2001, *ApJL*, 559, L97
- Giacconi R., Rosati P., Tozzi P., et al., 2001, *ApJ*, 551, 624
- Gilbertson W., Lehmer B., Doore K., et al., 2021, *arXiv*, arXiv:2112.03194

- Gilfanov M., MNRAS, 349, 146 (2004)
Gilfanov M., 2004, Progress of Theoretical Physics Supplement, 155, 49
Gilfanov M., Grimm H.-J., Sunyaev R., 2004, MNRAS, 351, 1365
Gilfanov M., Grimm H.-J., Sunyaev R., 2004, MNRAS, 347, L57
Gilfanov M., 2010, The Jet Paradigm, Lecture Notes in Physics, Volume 794. ISBN 978-3-540-76936-1. Springer-Verlag Berlin Heidelberg, p. 17
Gilfanov M., Merloni A., 2015, Space Science Reviews, Volume 183, Issue 1-4, pp. 121-148, doi: 10.1007/s11214-014-0071-5
Gladstone J. C., Copperwheat C., Heinke C. O., et al., 2013, ApJS, 206, 14
Grimm H.-J., Gilfanov M., Sunyaev R., 2002, A&A, 391, 923
Grimm H.-J., Gilfanov M., Sunyaev R., 2003, MNRAS, 339, 793
Grindlay J. E., Hertz P., Steiner J. E., Murray S. S., Lightman A. P., 1984, ApJL, 282, L13
Griffiths R. E., Padovani P., 1990, ApJ, 360, 483
Guo Q., White S., Boylan-Kolchin M., et al., 2011, MNRAS, 413, 101
Haberl F., Sturm R., Ballet J., et al., 2012, A&A, 545, A128
Helfand D. J., 1984, PASP, 96, 913
The HERA Collaboration, Abdurashidova Z., Aguirre J. E., Alexander P., Ali Z. S., Balfour Y., Beardsley A. P., et al., 2021, arXiv, arXiv:2108.02263
Hills, J. G. 1976, MNRAS, 175, 1P
Hornschemeier A. E., Brandt W. N., Garmire G. P., et al., 2000, ApJ, 541, 49
Hornschemeier A. E., Brandt W. N., Alexander D. M., et al., 2002, ApJ, 568, 82
Humphrey P. J., Buote D. A., 2008, ApJ, 689, 983
Ivanova N., Justham S., Ricker P., 2020, cee.book. doi:10.1088/2514-3433/abb6f0
Irwin J. A., 2005, ApJ, 631, 511
Juett A. M., 2005, ApJL, 621, L25
Kaaret P., Alonso-Herrero A., Gallagher J. S., et al., 2004, MNRAS, 348, L28
Kaaret P., Corbel S., 2009, ApJ, 697, 950
Kaaret P., Feng H., Roberts T. P., 2017, ARA&A, 55, 303
Kim D.-W., Fabbiano G., Trinchieri, G. 1992, ApJ, 393, 134
Kim D.-W. & Fabbiano G., ApJ, 611, 846 (2004)
Kim D.-W., Fabbiano G., Brassington N. J., et al., 2009, ApJ, 703, 829
Kim D.-W. & Fabbiano G., ApJ, 721, 1523 (2010)
Kim D.-W., Fabbiano G., Ivanova N., et al., 2013, ApJ, 764, 98
Kim, M. et al. ApJ., 814, 8
King A. R. et al., ApJ 552,109 (2001)
King A. R., 2002, MNRAS, 335, L13
Koering E., Falcke H., Markoff S., A&A, 382, L13 (2002)
Kolodzig A., Gilfanov M., Sunyaev R., Sazonov S., Brusa M., 2013, A&A, 558, A89
Kouroumpatzakis K., Zezas A., Sell P., et al., 2020, MNRAS, 494, 5967
Kovlakas K., Zezas A., Andrews J. J., et al., 2020, MNRAS, 498, 4790
Kremer K., Chatterjee S., Rodriguez C. L., Rasio F. A., 2018, ApJ, 852, 29
Kurczynski P., Gawiser E., Huynh M., et al., 2012, ApJ, 750, 117
Lehmer B. D., Brandt W. N., Alexander D. M., et al., 2007, ApJ, 657, 681
Lehmer B. at al. ApJ, 724, 559 (2010)
Lehmer B. D., Berkeley M., Zezas A., et al., 2014, ApJ, 789, 52
Lehmer B. D., Basu-Zych A. R., Mineo S., et al., 2016, ApJ, 825, 7
Lehmer B. D., Eufrasio R. T., Tzanavaris P., et al., 2019, ApJS, 243, 3
Lehmer B. D., Ferrell A. P., Doore K., et al., 2020, ApJS, 248, 31
Lehmer B. D., Eufrasio R. T., Basu-Zych A., et al., 2021, ApJ, 907, 17
Lewin, W. H. G., van Paradijs, I., van den Heuvel, E. P. J. (eds) 1995, X-ray Binaries, (Cambridge University Press: Cambridge)
Lewin, W. H. G. & van der Klis, M. 2006, Compact Stellar X-ray Sources, (Cambridge University Press: Cambridge)
Linden T., Kalogera V., Sepinsky J. F., et al., 2010, ApJ, 725, 1984

- Long K. S., van Speybroeck L. P., 1983, IN: Accretion-driven stellar X-ray sources (A84-35577 16-90). Cambridge and New York, Cambridge University Press, 1983, p.117
- Long K. S., van Speybroeck L. P., 1983, IN: Accretion-driven stellar X-ray sources (A84-35577 16-90). Cambridge and New York, Cambridge University Press, 1983, p.141
- Luo B., Fabbiano G., Strader J., et al., 2013, *ApJS*, 204, 14
- Madau P., Dickinson M., 2014, *ARA&A*, 52, 415
- Madau P., Fragos T., 2017, *ApJ*, 840, 39
- Mapelli M., Colpi M., Zampieri L., 2009, *MNRAS*, 395, L71
- Marchant P., Langer N., et al., 2017, *A&A*, 604, A55
- Mellema G., Koopmans L. V. E., Abdalla F. A., et al., 2013, *ExA*, 36, 235
- Miller J. M. et al., *ApJ*, 585, 37 (2003)
- Mineo S., Gilfanov M., Sunyaev R., *MNRAS*, 419, 2095 (2012)
- Mineo S., Gilfanov M., Sunyaev R., 2012, *MNRAS*, 426, 1870
- Mineo S., Rappaport S., Steinhorn B., Levine A., Gilfanov M., Pooley D., 2013, *ApJ*, 771, 133
- Mineo S., Gilfanov M., Lehmer B. D., Morrison G. E., Sunyaev R., 2014, *MNRAS*, 437, 1698
- Mineo S., Fabbiano G., D'Abrusco R., et al., 2014, *ApJ*, 780, 132
- Misra D., Fragos T., Tauris T. M., et al., 2020, *A&A*, 642, A174
- Norman C., Ptak A., Hornschemeier A., et al., 2004, *ApJ*, 607, 721
- Paolillo M., Puzia T. H., Goudfrooij P., et al., 2011, *ApJ*, 736, 90
- Peacock M. B., Zepf S. E., Maccarone T. J., et al., 2014, *ApJ*, 784, 162
- Peacock M. B., Zepf S. E., Kundu A., et al., 2017, *MNRAS*, 466, 4021
- Peacock M. B., Zepf S. E., 2016, *ApJ*, 818, 33
- Pooley D., Lewin W. H. G., Anderson S. F., et al., 2003, *ApJL*, 591, L131
- Popov S. B., Lipunov V. M., Prokhorov M. E., Postnov K. A., 1998, *ARep*, 42, 29
- Postnov K., *Astron. Lett.*, 29, 372 (2003)
- Poutanen J., Lipunova G., Fabrika S., et al., 2007, *MNRAS*, 377, 1187
- Predehl P., et al., 2021, *A&A*, 647, A1
- Prestwich A. H., Tsantaki M., Zezas A., et al., 2013, *ApJ*, 769, 92
- Prokopenko I. G., Gilfanov M. R., 2009, *AstL*, 35, 294
- Ptak A., Mobasher B., Hornschemeier A., et al., 2007, *ApJ*, 667, 826
- Ranalli P., Comastri A. & Setti G., *A&A*, 399, 39 (2003)
- Rappaport S. A., Podsiadlowski P., Pfahl E., 2005, *MNRAS*, 356, 401
- Reig P., 2011, *Ap&SS*, 332, 1
- Riley J., Agrawal P., Barrett J. W., et al., 2022, *ApJS*, 258, 34
- Sadowski A., Narayan R., 2016, *MNRAS*, 456, 3929
- Sazonov S., Khabibullin I., 2017, *MNRAS*, 466, 1019
- Sivakoff G. R., Jordán A., Sarazin C. L., et al., 2007, *ApJ*, 660, 1246
- Shakura N. I., Sunyaev R. A., 1973, *A&A*, 24, 337
- Shtykovskiy P., Gilfanov M., 2005, *A&A*, 431, 597
- Shtykovskiy P., Gilfanov M., 2005, *MNRAS*, 362, 879
- Shtykovskiy P., Gilfanov M., 2007, *AstL*, 33, 299
- Shtykovskiy P., Gilfanov M., 2007, *AstL*, 33, 437
- Soria R., Ghosh K. K., 2009, *ApJ*, 696, 287
- Strader J., Fabbiano G., Luo B., et al., 2012, *ApJ*, 760, 87
- Sunyaev R. A., Tinsley B. M., Meier D. L., 1978, *ComAp*, 7, 183
- Sunyaev R., Arefiev, V., Babyshkin, V., et al., 2021, *A&A*, 656, A132
- Swartz D. A., Soria R., Tennant A. F., Yukita M., 2011, *ApJ*, 741, 49
- Symeonidis M., Georgakakis A., Page M. J., et al., 2014, *MNRAS*, 443, 3728.
- Szuszkievicz E., Malkan M. A., Abramowicz M. A., 1996, *ApJ*, 458, 474
- Taam R. E., Sandquist E. L., 2000, *ARA&A*, 38, 113
- Tao L., Feng H., Grisé F., Kaaret P., 2011, *ApJ*, 737, 81
- Tauris T. M., van den Heuvel E. P. J., 2023, *pbse.book*
- Tzanavaris P., Georgantopoulos I., 2008, *A&A*, 480, 663
- Tzanavaris P., Fragos T., Tremmel M., et al., 2013, *ApJ*, 774, 136

- Verbunt F. & van den Heuvel E., 1995, In *X-ray binaries* (Cambridge University Press) p. 457
- van Speybroeck L., Epstein A., Forman W., et al., 1979, *ApJL*, 234, L45
- Voss R., Gilfanov M., 2007, *A&A*, 468, 49
- Voss R., Gilfanov M., 2007, *MNRAS*, 380, 1685
- Voss R., Gilfanov M., Sivakoff G. R., et al., 2009, *ApJ*, 701, 471
- Walton, D. J. 2018 et al., *ApJ*, 856, 128
- Weisskopf, M. C., Tananbaum, H. D., Van Speybroeck, L. P., et al., 2000, *Proc. SPIE*, 4012, 2
- Wiktorowicz G., Sobolewska M., Lasota J.-P., Belczynski K., 2017, *ApJ*, 846, 17
- Wolter A., Trinchieri G., 2004, *A&A*, 426, 787
- Zezas A., Fabbiano G., 2002, *ApJ*, 577, 726
- Zezas A., Hernquist L., Fabbiano G., Miller J., 2003, *ApJL*, 599, L73
- Zezas A., Fabbiano G., Baldi A., et al., 2007, *ApJ*, 661, 135
- Zhang W., Woosley S., Heger A., *ApJ*, 679, 639 (2008)
- Zhang Z., Gilfanov M., Voss R., et al., 2011, *A&A*, 533, A33
- Zhang Z., Gilfanov M., Bogdan A., *A&A*, 546, 36 (2012)
- Zhang Z., Gilfanov M., Bogdán Á., 2013, *A&A*, 556, A9.